Biogeotechnics 4 (2026) 100182

Contents lists available at ScienceDirect

Biogeotechnics

journal homepage: www.keaipublishing.com/en/journals/biogeotechnics/

Biopolymer amended kaolin for tailings containment: An engineered solution

Himanshu Yadav[a,b,*], Bharat Venkata Tadikonda[b,*]

[a] Department of Civil Engineering, Indian Institute of Technology Bombay, Mumbai, Maharashtra 400076, India
[b] Department of Civil Engineering, Indian Institute of Technology Guwahati, Guwahati, Assam 781039, India

ARTICLE INFO

Keywords:
Barriers
Diffusion
Hydro-chemo-mechanical behavior
Inorganic salts
Kaolin clay
Tailing disposal facilities
Xanthan gum

ABSTRACT

Tailing storage facilities contain mining waste with high-ionic-strength salts that might pose an environmental risk. Kaolin clays have recently received significant attention for barriers due to their reduced shrinkage cracking. Xanthan Gum, a biopolymer, has been studied to modify kaolin for use as a barrier to mitigate environmental issues. This study assesses the hydraulic, volume-change, diffusion, and retardation properties of kaolin clay and xanthan gum-modified kaolin under hydro-chemo-mechanical loading relevant to mine storage applications. Through-diffusion experiments were performed on materials acquired from hydraulic permeation testing under mechanical stress to replicate field conditions. Xanthan gum improved chemical compatibility, reduced hydraulic infiltration, and lowered diffusion rates considerably. Theoretical concentration profiles for kaolin and xanthan gum-amended kaolin barriers were derived using numerical modelling of the advection-diffusion equation utilizing the finite difference method. This study indicates that xanthan gum-modified kaolin is a feasible, environmentally sound option for improving the efficacy of barriers in mine tailing disposal, presenting considerable promise for mitigating the environmental effect of tailings storage facilities.

1. Introduction

Mine tailings are the residual waste produced during the extraction of metals, minerals, and non-renewable energy sources like coal and fossil fuels (Mäkinen et al., 2020). Approximately 97%–99% of treated ore is transformed into tailings with high moisture content. The leachate from coal combustion products (CCPs) comprises elevated Na^+, K^+, Ca^{2+}, and Mg^{2+} (Chen et al., 2019). The leachate produced from red mud/bauxite and copper tailings has elevated levels of inorganic cations, sulfates, and chlorides (Hu & Zhang, 2023; Li & Rowe, 2020). Likewise, the leachate from dolomite and limestone tailings has elevated levels of calcium ions (Farmaki et al., 2018; Harwood & Koirtyohann, 1987), whereas potash mining results in tailings with substantial amounts of sodium and potassium ions (Tallin et al., 1990). Mining wastes are disposed of as slurry in designed disposal facilities behind dams (Akhila & Bharat, 2022; Yin et al., 2020). The leachate produced from the tailings poses an environmental risk due to the spreading of contaminants into the surrounding environment (Abreu et al., 2016; Concas et al., 2006; García-Giménez & Jiménez-Ballesta, 2017; Parviainen, 2009; Singh et al., 2023). The engineering barrier is an essential component of tailing disposal systems, designed to inhibit the movement of these contaminants into the environment (Fig. 1A).

The engineered barriers are also exposed to mechanical stress due to the weight of the tailing material in the tailing disposal facility. The volume change as well as the hydraulic performance of kaolin depends on the various surface and chemo-mechanical forces. The hydraulic performance of barriers is more critical at lower mechanical loads (Das & Bharat, 2021). Most engineered barrier systems require low hydraulic conductivity ($< 10^{-9}$ m/s). A low value of hydraulic conductivity is a necessary but not sufficient condition for the long-term performance of barriers (Devlin & Parker, 1996; Ruffing et al., 2018; Sample-Lord et al., 2021). At lower hydraulic permeation, diffusion can be a significant contaminant mechanism and should be considered in practice (Choi et al., 2015; Takai et al., 2017). High attenuation capacity or high sorption ability of the liner is required for engineered barriers, which can be fulfilled by amendment of the base material with activated carbon, zeolite, or bentonite (Hong & Shackelford, 2017; Malusis et al., 2010). The containment of tailing waste is not much different from the containment of landfill waste. The design of landfill liners considers the diffusion and adsorption parameters apart from hydraulic conductivity.

* Corresponding authors.
E-mail addresses: yadav.himanshu1234@gmail.com, himanshu.yadav@iitb.ac.in (H. Yadav), tvb@iitg.ac.in (B.V. Tadikonda).

https://doi.org/10.1016/j.bgtech.2025.100182
Received 16 January 2025; Received in revised form 27 March 2025; Accepted 24 April 2025
Available online 26 April 2025
2949-9291/© 2026 The Authors. Publishing services by Elsevier B.V. on behalf of KeAi Communications Co. Ltd. This is an open access article under the CC BY-NC-ND license (http://creativecommons.org/licenses/by-nc-nd/4.0/).

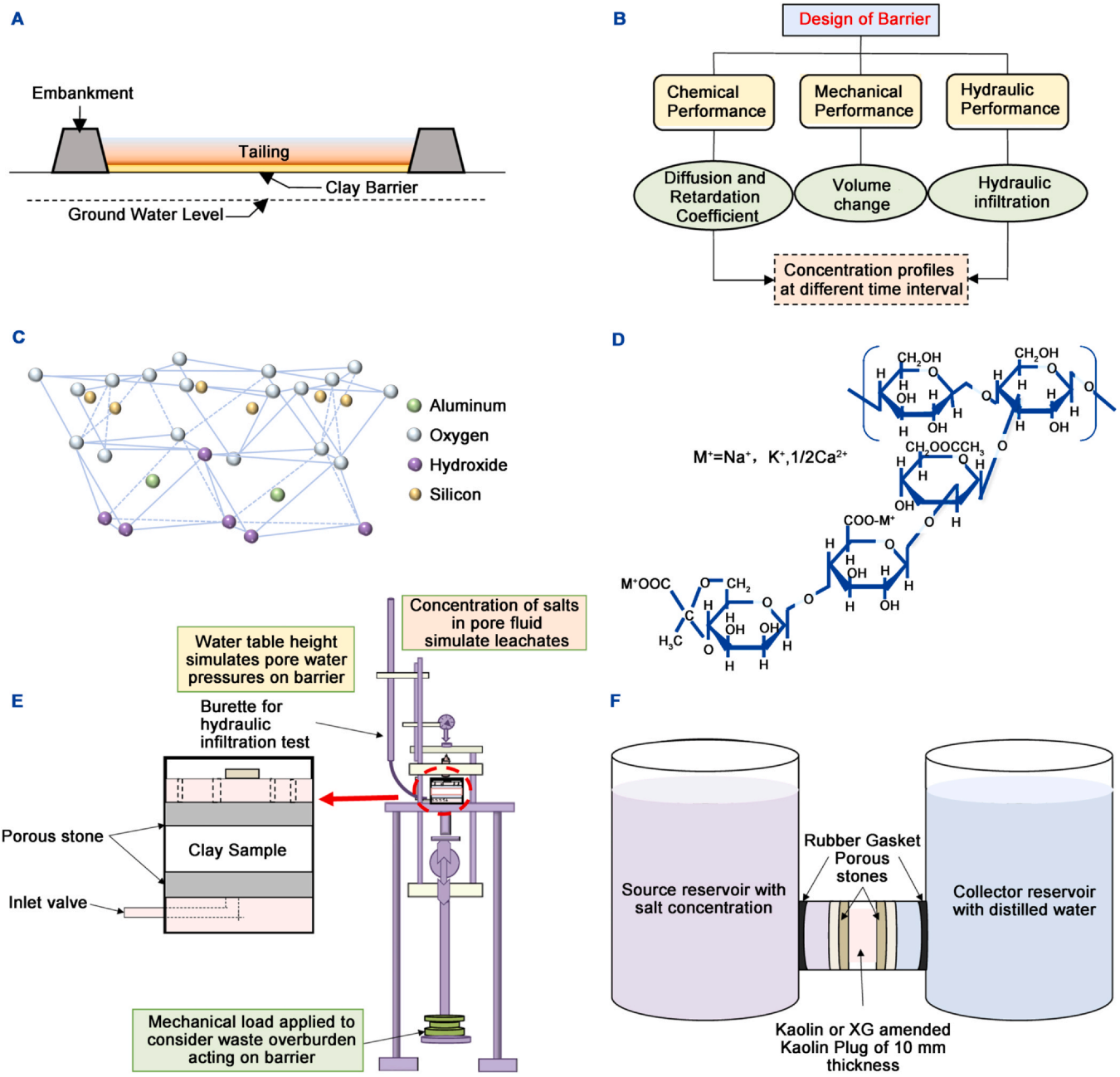


Fig. 1. (**A**) Schematic diagram for tailing disposal facility with clay liner; (**B**) The conceptual diagram for design of engineered barriers; (**C**) Illustration showing the basic structure of Kaolinite mineral after (Grim, 1959); (**D**) Chemical structure of Xanthan gum after (Adhikary & Singh, 2004); Experimental setup for (**E**) hydro-chemo-mechanical performance of kaolin and xanthan gum amended kaolin samples; and (**F**) through diffusion experimental setup.

But such practices are currently lacking in the barrier design of tailing disposal facilities, and these important aspects should also be included in the tailing disposal facilities. The hydraulic, chemical, and mechanical performance of the material is of great importance for using it as an engineered barrier, as shown in Fig. 1B. The hydraulic infiltration rate of the material is important to arrest the advective flows. The diffusion and retardation characteristics of the barrier material are important to retain and prevent the migration of contaminants. The volume change characteristics of barrier materials are important to understand the collapsing nature of the barrier, which can cause distress to the cover system.

Active clays such as bentonites are commonly used as barriers due to their very low saturated hydraulic conductivity, high sorption, high self-sealing ability, and low diffusion ability (Benson et al., 1994; García-Guzmán et al., 2023; Kaufhold et al., 2015). The saturated hydraulic conductivity of bentonite lower than 1×10^{-9} m/s results in minimal advective flow of the contaminants (Darde et al., 2021; Das & Bharat, 2017; Yadav & Bharat, 2022; Yu et al., 2020). Thus, diffusion is the dominant contaminant transport mechanism across the barrier due to the low value of hydraulic conductivity. Although the performance of bentonite is extremely outstanding under low-concentration salts and some heavy metal contaminants, it loses its self-sealing ability under the influence of high-ionic-strength salts due to loss of osmotic potential. (Christian & Tarek, 2021; Das & Bharat, 2021; Li & Rowe, 2020; Setz et al., 2017; Yadav & Tadikonda, 2022). Further, the bentonite clay shows high shrinkage cracks, when subjected to the number of wetting and drying cycles and the presence of cracks in these barrier materials favors the advection dominant flows of contaminants. Thus, the barrier performance under high-ionic-strength salt solutions is critical in containing different waste contaminants (Das & Bharat, 2017).

Kaolin clay is a non-active clay dominated by kaolinite minerals and exhibits contrasting behavior with that of bentonite under the influence of extreme salt conditions. Kaolinite mineral consists of silica and alumina sheets joined together in a 1:1 layered arrangement. The silica sheet consists of Si^{4+} at the center and O^{2-} at the edges. The alumina sheet consists of Al^{3+} at the center and OH^- at the corners (Anam et al., 2023). The kaolinite mineral has O^{2-} termination sites towards the silica face and OH^- sites towards the alumina face, while termination sites of the edges contain both OH^- and O^{2-} as shown in Fig. 1C (Grim, 1959; Yadav et al., 2023). The kaolinite mineral contains pH-dependent charges due to the reactive nature of termination sites at edges and the alumina basal surface (Celik, 2004). Although the kaolin, compacted at high density, exhibits swelling under low inundation stresses, it exhibits collapse at low compaction density (Choudhury & Bharat, 2018). The presence of high ionic strength salt solutions improves the osmotic efficiency of the kaolin during inundation. Further, kaolin contains uniform morphology and exhibits no crack upon drying, even in the presence of different pore fluids (Mishra et al., 2019). A protective layer of kaolin at a high density (1.7 mg/m^3) over the GCL was used to arrest the contaminant migration through the GCL under high ionic strength salt solutions in the study conducted by Das and Bharat (Das & Bharat, 2021). However, the effort required to compact the kaolin to such a high density is quite high. Moreover, kaolin is not explored much for barrier applications, although kaolin is a largely available natural clay mineral across the globe. Further, the availability of the bentonite clay is difficult in certain regions, including the North Eastern region of India, while this region has a large quantity of kaolin clay. Due to the desirable crack-resistant characteristics of kaolin, it should be explored as a potential material for engineered barriers along with some amendments, as kaolin alone is poor in sealing ability, specific surface area, cation exchange capacity, and exhibits a higher hydraulic conductivity and diffusion coefficient.

Biopolymers such as xanthan gum (XG), Guar gum, Gellan gum, and sodium alginate have been widely used in recent times to improve soil characteristics, as these polymers are environmentally friendly and have a very low carbon footprint (Amulya et al., 2021; Elkenawy et al., 2023). The XG forms a thick and viscous gel upon hydration due to the presence of carboxyl groups, which makes it a hydrophilic biopolymer, as shown in the basic structure of the XG shown in Fig. 1D (Adhikary & Singh, 2004). It is shown that the shear strength of the natural soil improved significantly with the addition of xanthan gum (Ni et al., 2024) and reduced hydraulic conductivity by several orders (Chang et al., 2015; Dehghan et al., 2019; Kumar & Sujatha, 2021). The XG is utilized as a sustainable binder material for the improvement of the California bearing ratio (CBR) of soils in pavement applications (Elkafoury & Azzam, 2021). Similarly, the utilization of XG for stabilizing slope with clayey as well as sandy loam soil was found to be very effective (Ding & Geng, 2025; Wan et al., 2024). The XG is also effective for soil stabilization against the Freeze thaw cycles (Bozyigit et al., 2023; Bozyigit, 2025). Several biopolymers-amended soil materials are successfully used to remove contaminants from the water (El-Sherbiny et al., 2013).

The XG is highly stable and does easily degrade in soil environment due unavailability of microorganisms that can degrade XG (Biju & Arnepalli, 2020; Cadmus et al., 1982; Fu et al., 2022). These biopolymers are stable over a wide pH range of 2–11 (Rosalam & England, 2006). Further, the amount of overburden pressure in mine tailing facilities goes up to 700 kPa during the closure of the facility (Peirce et al., 1986; Yadav & Tadikonda, 2022). This high overburden pressure significantly reduces the fluid permeation rates (Das & Bharat, 2021), due to the achievement of higher density in clay liners under such loading situations. The fluid permeation rates under lower pressures, which means during the initial period of service are crucial. The XG can perform during the initial period of service, and long-term performance will be taken care of by the kaolin in the worst case of biodegradation of these biopolymers. The volume change, hydraulic, and diffusion behavior of XG-amended kaolin are not currently available. Further, there is no study available on the hydraulic performance of XG-amended clays under hydro-chemo-mechanical loading conditions for barrier applications. Similarly, there is no study available on the diffusion parameters of biopolymer-amended kaolin. But such studies are of great interest for arresting the contaminants from environmental pollution. The present study aims to develop a novel engineered barrier material for tailing disposal facilities from natural kaolin and a biopolymer (XG). The objectives of the current study are

- To evaluate the applicability of kaolin and XG-amended-kaolin (XGK) to improve the chemical compatibility under different chemo-mechanical loading conditions. The tests are conducted with three different high-ionic-strength salts that are encountered in mine tailing waste disposal facilities under critical mechanical loading of 20 kPa.
- To evaluate the diffusion and retardation characteristics of three salts for kaolin and XGK.
- To evaluate the fate of three different contaminants (i.e., Na^+, K^+, and Ca^{2+}) through a 500 mm thick barrier of kaolin and XGK and evaluate the design periods of the tailing disposal facilities.

2. Materials and methodology

2.1. Materials

Kaolin. The kaolin used in the current study was commercially procured without any pretreatment. The basic index and surface properties of kaolin are reported in Table 1.

Xanthan Gum. Xanthan gum (XG) is a polysaccharide, a variety of biopolymers produced from microbial activity. The biopolymer is highly soluble in water and produces a thick and viscous gel. It is an anionic biopolymer and contains various $-COO^-$ and $-OH^-$ groups (Chakraborty et al., 2023). The presence of the carboxyl group makes the xanthan gum hydrophilic and increases its ability to form complexes with cations.

Permeated fluids. Sodium, potassium, and calcium chlorides with 99% purity, procured from Spectrochem (India), were used to make 0.5 mol/L solutions. The required amount of salt was mixed with distilled water in the volumetric flask to prepare the salt solutions. Distilled water was also used as a pore-fluid, along with different salt solutions.

2.2. Methodology

Hydro-chemo-mechanical behavior. Hydraulic and volume change behavior of compacted kaolin and XGK was studied using a modified oedometer setup as shown in Fig. 1E. The oedometer was modified by providing the provision for connecting a burette for measuring hydraulic flux (Yadav et al., 2022). The modified setup was fabricated from a solid perspex cylinder to accommodate a soil sample of 53 mm diameter and 10 mm thickness. A 5 mm thick porous stone was provided on either side of the compacted sample. A 42-grade filter paper

Table 1
Index and surface properties of studied kaolin.

Properties	Values	Standards
Specific Gravity	2.62	IS 2720–3–2
Liquid limit	40	IS 2720–5 (IS: 2720, 1985)
Plastic limit	32	ASTM standard D4318–10, 2010
Shrinkage limit	28	Clod test (Gapak et al., 2017)
Total CEC, (meq/100 g)	5	Chapman, 1965
Specific Surface Area, S_A (m^2/g)	11	N_2 gas adsorption technique (Klute & Dinauer, 1986).

was used in between the compacted sample and porous stone to prevent clogging of the porous stone. The samples of kaolin without any amendment and XGK were independently compacted at an air-dried density of 1.2 mg/m^3. The test set-up with compacted kaolin and XGK was placed on the loading assembly separately. The set-up was connected to the dial gauge to measure vertical strain at the top of the compacted sample. The burette with the desired pore-fluid was connected from the bottom of the compacted sample, with the valve of the burette kept closed until the start of the experiment. A load of 20 kPa was applied to the compacted sample to simulate the weight of sediments present in tailing disposal facilities on the engineered barrier system. The valve of the burette was opened to allow the flow of pore fluid through the compacted sample. The hydraulic infiltration rates of pore-fluid were continuously estimated by monitoring the outflow in the burette. The test was continued until the hydraulic infiltration rates and dial gauge readings were constant for 24 hours. The hydraulic infiltration rate at equilibrium is saturated hydraulic conductivity. The hydraulic infiltration rates are a measure of the sealing ability of compacted samples. The hydraulic infiltration rate lower than 1×10^{-9} m/s represents the complete sealing of macro-voids in modified kaolin samples. The time required to achieve the hydraulic infiltration rate slower than 1×10^{-9} m/s known as sealing time (ST). The dial gauge readings provide the volume change of the compacted sample, which was represented in terms of normalized thickness (h/h_0). The tests were conducted using a high concentration of three common salt solutions in tailings. The hydraulic, sealing, and volume change abilities of both kaolin and XGK samples were evaluated under chemo-mechanical loading conditions.

Diffusion behavior. The laboratory through-diffusion experiments of compacted kaolin and XGK were performed under high ionic solutions of NaCl, KCl, and $CaCl_2$. The diffusion cell was fabricated from a solid perspex cylinder to accommodate a sample of 24 mm in diameter and 10 mm in thickness, as shown in Fig. 1F. The diffusion setup should have each dimension greater than 6 times the size of the clay particle. So, this criterion is being satisfied considering a 10 mm width and 24 mm diameter for the setup. A higher width of the sample can increase the saturation time for XGK samples due to low hydraulic conductivity. So, a width of 10 mm and a 24 mm diameter was selected for the setup fabrication. The samples for diffusion experiments were obtained from the permeation experiment to simulate the field conditions. The barrier is subjected to mechanical loading conditions due to the self-weight of the tailing sediments in the tailing disposal facility. The migration of contaminants also depends on the mechanical loading conditions subjected to the barrier material. To consider the influence of the loadings on the diffusion, the test has been performed under field conditions. The kaolin and XGK samples were initially compacted at a density of 1.2 mg/m^3 for the hydro-mechanical test set-up with 15 mm thickness and permeated with distilled water for saturation of the sample under mechanical loading. The sample was taken out upon complete saturation of compacted kaolin and XGK; Saturation was ensured when hydraulic conductivity and dial gauge readings were constant over 24 hours. The sample was dismantled carefully, and a saturated sample for the diffusion test was extracted from this sample with the help of a sharp annular ring of 24 mm diameter. The thickness of the extracted sample was maintained at 10 mm, and the excess sample was trimmed off using a sharp knife. The obtained saturated sample was placed inside the diffusion cell for the through-diffusion experiment (Yadav & Bharat, 2022). The diffusion cell was connected to two reservoirs on either end. The source reservoir was filled with the desired salt solution of the required concentration and the collector reservoir was filled with distilled water. The concentrations of source and collector reservoirs were monitored periodically to obtain the concentration variations with time. The diffusion coefficient and retardation factors are simultaneously evaluated from the measured temporal ion concentrations by inverse analysis of the governing diffusion equation along with appropriate boundary conditions.

Microstructural analysis. The morphology of xanthan gum, kaolin, and XGK samples was captured by field emission scanning electron microscopy (FESEM), Zeiss, Gemini 300. The FESEM micrographs of kaolin and XGK samples were also obtained after permeation with different pore fluids. These samples were collected after the permeation experiment with distilled water, 0.5 mol/L NaCl, 0.5 mol/L KCl, and 0.5 mol/L $CaCl_2$ as the pore fluid. Kaolin and XGK samples were kept for freeze-drying to remove the moisture without any changes in the structure/fabric. The samples were placed on a double-sided carbon tape and gold-coated before taking the micrographs. Micrographs were collected for all the samples. Similarly, the elemental composition of kaolin samples, xanthan gum, and XGK samples after permeation with different pore fluids was also performed.

The samples for the AFM were prepared using drop-casting on the glass surface. The kaolin and XGK samples were dissolved in distilled water in a solid: liquid ratio of 1:1000. The samples were then drop-cast and dried at 105 ℃ overnight. The morphology and roughness of both samples were captured using Cypher, Oxford, UK. Surface area and pore size analysis of kaolin and XGK were done on dry samples by N_2 adsorption at 77 K using Quantachrome-Autosorb-IQ MP, USA.

3. Theoretical background

The governing advection-diffusion equation for studying contaminant transport through saturated soils is given by (Bharat et al., 2009):

$$\frac{\partial C}{\partial t} = \left(\frac{D_e}{R_d}\right)\frac{\partial^2 C}{\partial x^2} - \left(\frac{V_s}{R_d}\right)\frac{\partial C}{\partial x} \tag{1}$$

The transport of contaminants is governed by Fick's diffusion equation (Eq. 2) in the absence of advection (Bharat, 2013; Shackelford et al., 1989; Shackelford, 1991; Yadav & Bharat, 2022):

$$\frac{\partial C}{\partial t} = \left(\frac{D_e}{R_d}\right)\frac{\partial^2 C}{\partial x^2} \tag{2}$$

Where C is the concentration of contaminant (salt) at time t (s) and spatial location x (cm); V_s is the seepage velocity; and R_d is the dimensionless retardation factor, is given by (Eq. 3).

$$R_d = 1 + \frac{K_d \rho_d}{n} \tag{3}$$

Where K_d is the partition coefficient, ρ_d is the dry bulk density of soil and n is the porosity of the soil.

The initial conditions for the laboratory diffusion test are given by (Bharat et al., 2009).

$$C(x = 0,\ t = 0) = C_0 \tag{4a}$$

$$C(x,\ t = 0) = 0 \tag{4b}$$

$$C(x = L,\ t = 0) = 0 \tag{4c}$$

Eq. 4 represents the concentration of salts in the source, concentration along the sample, and collector reservoir. The boundary conditions at the source and collector reservoir are given by (Bharat et al., 2009; Das & Bharat, 2017):

$$C(x = 0,\ t) = C_0 + \frac{nD_e}{H_s}\int_0^t \left(\frac{\partial C}{\partial x}\right)_{x=0} dt \tag{5}$$

$$C(x = L,\ t) = -\frac{nD_e}{H_c}\int_0^t \left(\frac{\partial C}{\partial x}\right)_{x=L} dt \tag{6}$$

Where C_0 is the initial concentration of contaminants at $t = 0$, H_s and H_c are equivalent heights of source and collector reservoirs, respectively.

Estimation of diffusion coefficient, D_e, and retardation factor, R_d, is important for engineered barrier design. The diffusion equation, Eq. (2)

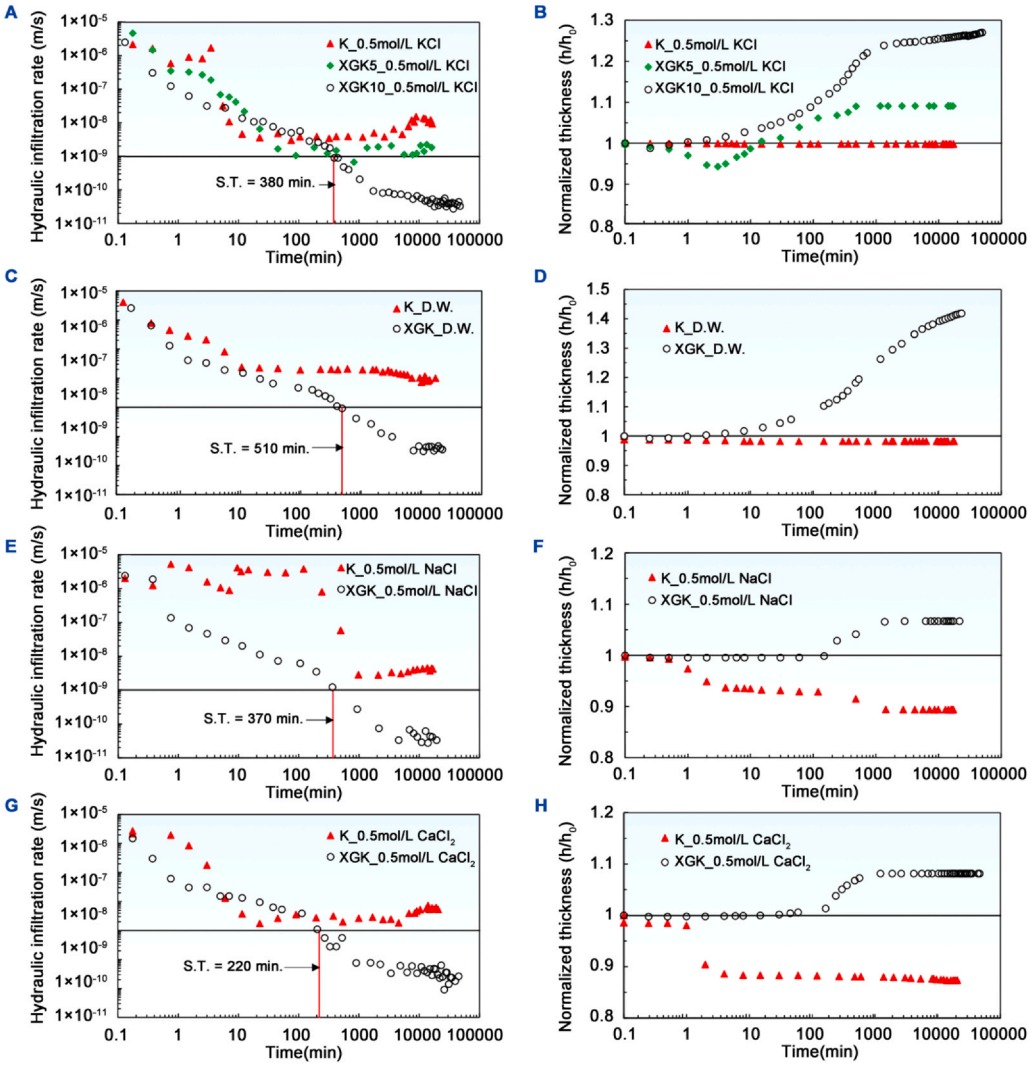


Fig. 2. Temporal variations of (A, C, E, G) hydraulic infiltration rates for kaolin and XGK with: (**A**) 0.5 mol/L KCl, (**C**) Distilled water, (**E**) 0.5 mol/L NaCl, and (**G**) 0.5 mol/L $CaCl_2$ under 20 kPa mechanical loading; Temporal variations of (B, D, F, H) normalized thicknesses for kaolin and XGK with (**B**) 0.5 mol/L KCl; (**D**) Distilled water; (**F**) 0.5 mol/L NaCl; and (**H**) 0.5 mol/L $CaCl_2$ as pore fluid under 20 kPa mechanical loading.

was solved along with initial and boundary conditions (Eqs. 4–6) to obtain a closed-form analytical solution (Bharat, 2013). The barrier design parameters were estimated by minimizing the errors between experimental and theoretical concentrations by solving forward analysis using the modified particle swarm optimization technique (Bharat et al., 2009). The design parameters were estimated for both kaolin and XGK under high-concentration salt environments.

The values of diffusion coefficient, retardation factor, and seepage velocity were evaluated experimentally for kaolin as well as XGK samples and were used for numerical analysis. The migration of the contaminants depends on advection flow for kaolin alone, while it is governed by the diffusion mechanism for XGK. The movement of contaminants through both kaolin and XGK can be considered using the combined advection-diffusion equation. To obtain the concentration profiles with time for different cations, the partial differential equation (Eq.1) was solved using the forward time central space (FTCS) scheme of finite difference method using MATLAB, the discretized form of Eq. 1 is presented as follows:

$$\frac{C_i^{j+1} - C_i^t}{\Delta t} = \frac{D_e}{R_d}\left(\frac{C_{i+1}^j - 2C_i^j + C_{i-1}^j}{\Delta x^2}\right) - \frac{V_s}{R_d}\left(\frac{C_i^j - C_{i-1}^j}{\Delta x}\right) \quad (7)$$

which can be presented as:

$$C_i^{j+1} = C_i^t + \frac{D_e \Delta t}{R_d \Delta x^2}(C_{i+1}^j - 2C_i^j + C_{i-1}^j) - \frac{V_s \Delta t}{R_d \Delta x}(C_i^j - C_{i-1}^j) \quad (8)$$

Finally, concentration profiles for 500 mm thick barrier material were obtained and design life with different cations was estimated.

4. Results and discussion

4.1. Hydraulic and volume change behaviour

A different percentage of biopolymer amendments was explored. A 5% (XGK5) and 10% XG (XGK10) by weight were considered with the kaolin for evaluating the performance. The temporal variations of hydraulic infiltration rates for kaolin, XGK5, and XGK10 under 20 kPa mechanical load with 0.5 mol/L KCl as pore-fluid were presented in Fig. 2A. The hydraulic infiltration rate of the kaolin sample was found to be higher initially up to 4 minutes, but subsequently reduced from 2×10^{-6} to 4.7×10^{-9} m/s within 10 minutes from the start of the experiment. The hydraulic infiltration rate did not change significantly further with time and could not attain the limiting value of 1×10^{-9} m/s. The initial sudden drop in the hydraulic infiltration rate is due to changes in the fabric of kaolin from dispersed to flocculated upon inundation (Choudhury & Bharat, 2018). The hydraulic infiltration rate of

XGK5 was found to be 2.53×10^{-6} m/s initially, but subsequently reduced with time. The hydraulic infiltration rate of XGK5 decreased, but it could not achieve the limiting value. Whereas, the hydraulic infiltration rate of the XGK10 decreased gradually and achieved the limiting value of hydraulic infiltration rate in 380 minutes from the start of the experiment, as shown in Fig. 2A. The XGK10 sample attained an equilibrium hydraulic infiltration value of $10^{-10} - 10^{-11}$ m/s after 3000 minutes from the start of the experiment. A reduction of hydraulic infiltration rate by two to three orders of magnitude was observed due to the amendment with the 10% XG. The reason behind the reduction in hydraulic infiltration of XGK is the clogging of pores with xanthan gum gel. The rate of reduction of hydraulic infiltration is quicker in kaolin as compared to XGK, because the changes in fabric structure of kaolin do not take much time as compared to the formation of XG gel.

The volume change behavior of kaolin, XGK5, and XGK10 in terms of normalized thickness with 0.5 mol/L KCl as pore–fluid was plotted in Fig. 2B under 20 kPa mechanical load. Normalized thickness (h/h_0) is defined as the ratio of the present thickness of the sample to the initial thickness. A collapse of the kaolin sample was observed due to the application of the prevailing hydro-mechanical loading conditions. The normalized thickness of the kaolin sample did not increase after the initial collapse, which represents the insignificant development in DDLs of the kaolin sample. The XGK5 sample showed an initial collapse of 5% during the application of chemo-mechanical loading. Further, the XGK5 sample showed swelling and achieved an equilibrium normalized thickness of 1.08, which represents the overall swelling of the sample due to the formation of XG gel. For the XGK10 sample, a slight collapse of approximately 1% was initially observed due to the application of hydro-mechanical load. The sample achieved its original volume within 1 minute of the start of the experiment, and it started further swelling with time due to the complete formation of XG gel. An equilibrium normalized thickness of 1.27 was achieved with XGK10, which represents the overall swelling of the sample. The swelling of XGK samples is taking place due to a higher swelling pressure than the applied stress. The swelling of the sample upon inundation with 0.5 mol/L KCl solution is attributed to the formation of XG gel. The XG gel interacts with potassium ions due to electrostatic interaction between the carboxyl groups of XG and cations. The hydraulic and volume change behaviour of samples were checked with different percentages of the XG. As the lower percentages of the XG are not able to seal the macro-voids in kaolin and resulted in a higher fluid permeation rate than limiting value was observed with 5% XG, higher amount of XG (i.e., 10%), was only considered for further testing.

The temporal variations of hydraulic infiltration rates for kaolin and XGK10 under 20 kPa mechanical load with distilled water (D.W.) as pore-fluid were presented in Fig. 2C. The hydraulic infiltration rate of the kaolin sample was found to be higher at the beginning of the test, but subsequently reduced from 4×10^{-6} to 1.5×10^{-8} m/s within 10 minutes from the start of the experiment. The hydraulic infiltration rate did not change significantly further with time and could not attain the limiting value of 1×10^{-9} m/s. The initial sudden drop in the hydraulic infiltration rate is due to changes in the fabric of kaolin from dispersed to flocculated upon inundation (Choudhury & Bharat, 2018). The hydraulic infiltration rate of XGK10 was also plotted in the same figure. The hydraulic infiltration rate was found to be 2.55×10^{-6} m/s at the start of the experiment, which reduced with time. The hydraulic infiltration rate of the XGK decreased gradually and achieved the limiting hydraulic infiltration rate 510 minutes from the start of the experiment, as shown in Fig. 2C. The XGK sample attained an equilibrium hydraulic infiltration value of 3.5×10^{-11} m/s after 8000 minutes from the start of the experiment. A reduction of three orders of magnitude in hydraulic infiltration rate was observed in the values before and after its amendment with XG.

The volume change behavior of kaolin and XGK in terms of normalized thickness with distilled water as pore-fluid was plotted in Fig. 2D under mechanical load. A collapse of the kaolin sample was observed due to the application of prevailing hydro-mechanical loading conditions. Kaolin hydration with distilled water results in the alteration of charges on its edges from positive to negative, which nullifies the coulombic attraction between the edges and faces of kaolin particles (Choudhury & Bharat, 2018; Das & Bharat, 2021). The normalized thickness of the kaolin sample did not increase after the initial collapse, which represents the development of thinner diffused double layers (DDLs) of the kaolin sample (Das & Bharat, 2021; Puppala et al., 2017). For XGK10, a slight collapse of approximately 1% was initially observed due to the application of hydro-mechanical load. The sample achieved its original volume within 2 minutes of the start of the experiment, and it started further swelling with time due to the complete formation of xanthan gum gel. An equilibrium normalized thickness of 1.41, which represents the overall swelling, was achieved with XGK10. The XG in the voids of kaolin sorbs pore-fluid, and leads to the swelling of the samples, which was also observed by earlier researchers (Kwon et al., 2023). The swelling of XGK10 is thus taking place due to a higher osmotic pressure between XG gel than the applied stress.

The temporal variations of hydraulic infiltration rates for kaolin and XGK10 under 20 kPa mechanical load with 0.5 mol/L NaCl as pore fluid were presented in Fig. 2E. The hydraulic infiltration rate of the kaolin sample was found to be higher at the beginning of the experiment up to 200 minutes, but subsequently reduced from 3×10^{-6} to 3×10^{-8} m/s within 600 minutes from the start of the experiment. The equilibrium value of the hydraulic infiltration rate varied between 10^{-8} and 10^{-9} m/s. The hydraulic infiltration rate did not change significantly further with time and could not attain the limiting value of 1×10^{-9} m/s. The sudden drop in the hydraulic infiltration rate was due to changes in the fabric of kaolin from dispersed to flocculated upon inundation. The hydraulic infiltration of the XGK10 sample was also plotted in the same figure. The hydraulic infiltration rate was found to be 2.4×10^{-6} m/s initially, which reduced with time. The hydraulic infiltration rate of the XGK10 decreased gradually and achieved the limiting hydraulic infiltration rate of 10^{-9} m/s after 370 minutes from the start of the experiment, as depicted in Fig. 2E. The XGK10 sample attained an equilibrium hydraulic infiltration rate of $5 \times 10^{-10} - 3.3 \times 10^{-11}$ m/s after 6000 minutes from the start of the experiment. A reduction of hydraulic infiltration rate by two orders of magnitude was observed due to amendment with the XG.

The volume change behavior of kaolin and XGK in terms of normalized thickness with 0.5 mol/L NaCl as pore-fluid was plotted in Fig. 2F for a 20 kPa mechanical load. A collapse of 12% for the kaolin sample was observed due to the application of hydro-mechanical loading conditions. The normalized thickness of the kaolin sample did not increase after the collapse, which represents the development of thinner DDLs of the kaolin due to low surface charge density (Das & Bharat, 2021; Puppala et al., 2017). For XGK10, a slight collapse of approximately 1% was initially observed due to the application of hydro-mechanical load. The sample achieved its original volume within 100 minutes from the start of the experiment, and it started further swelling with time due to the formation of xanthan gum gel. An equilibrium normalized thickness of 1.06 was achieved with XGK, which represents the overall swelling of the sample. The swelling of XGK is taking place due to a higher osmotic repulsive pressure between XG gel than the applied load. The swelling of the sample upon inundation with 0.5 mol/L NaCl is attributed to the formation of XG gel. The XG gel formed with water molecules interacts with sodium ions due to electrostatic attraction from the carboxyl group in XG.

The temporal variations of hydraulic infiltration rates for kaolin and XGK10 under mechanical load with 0.5 mol/L $CaCl_2$ as pore-fluid were presented in Fig. 2G. The hydraulic infiltration rate of the kaolin sample was found to be higher at the beginning of the test, but subsequently reduced by orders of magnitude within 20 minutes from the start of the experiment. The hydraulic infiltration rate did not change significantly further with time and could not attain the limiting value of 1×10^{-9}

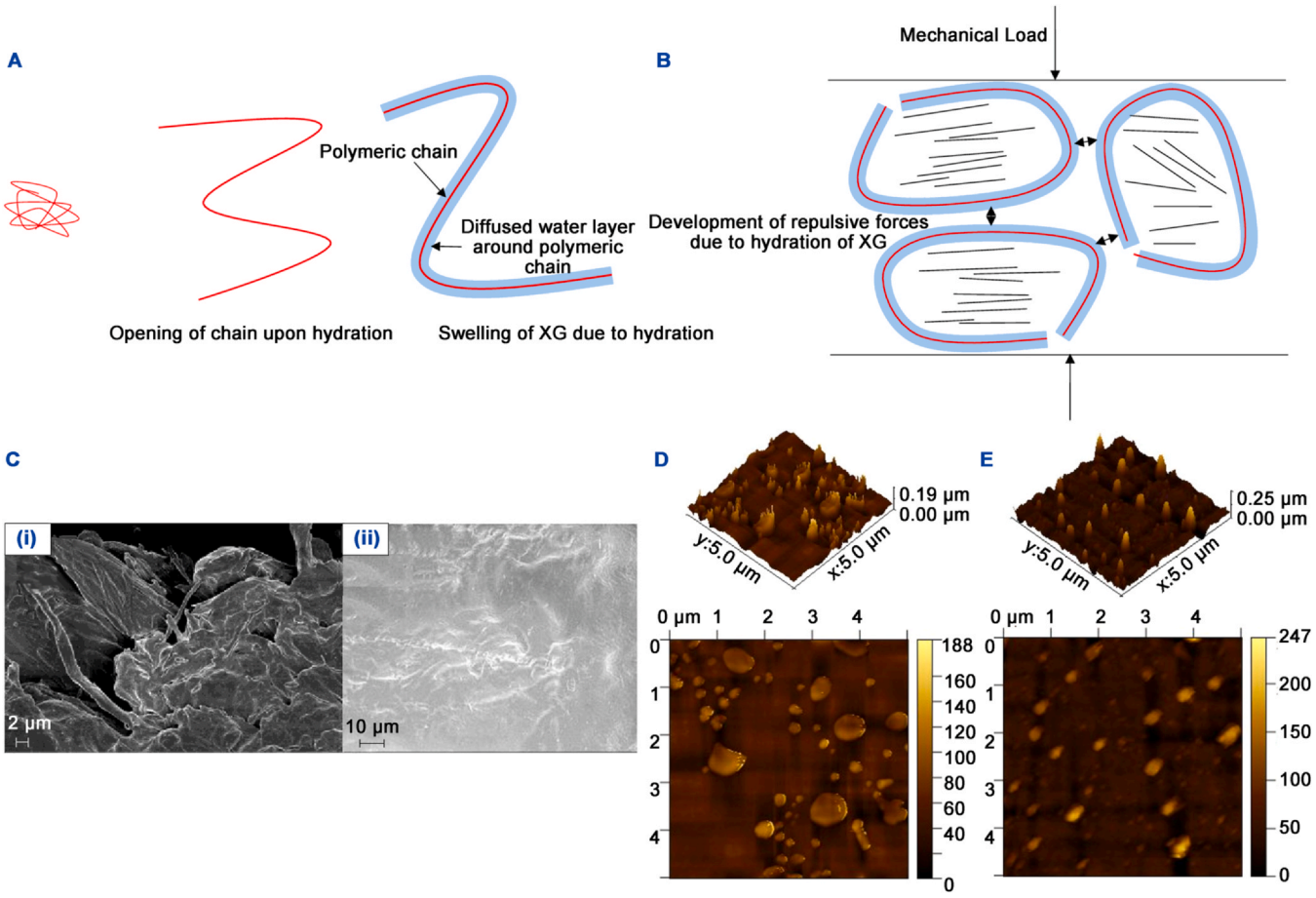


Fig. 3. (**A**) Hydration mechanism of XG; (**B**) Development of repulsive forces in XGK due to XG gel formation; (**C**) FESEM micrograph of XG in (i) dry powdered state, (ii) coating formed after hydration; AFM images of (**D**) kaolin; and (**E**) XG amended kaolin.

m/s. The initial drop-in hydraulic infiltration rate is due to the changes in the fabric of kaolin from dispersed to flocculated upon inundation (Choudhury & Bharat, 2018). The hydraulic infiltration rate of XGK10 was also plotted in Fig. 2G. The hydraulic infiltration rate was initially on the order of 1.5×10^{-6} m/s, which reduced with time. The hydraulic infiltration rate of the XGK10 decreased gradually and achieved the limiting value of hydraulic infiltration rate in 220 minutes from the start of the experiment, as shown in Fig. 2G. The XGK10 sample attained an equilibrium hydraulic infiltration rate of 3×10^{-11} m/s after 2000 min from the start of the experiment. A reduction of equilibrium hydraulic infiltration rates by two to three orders of magnitude was observed due to in of kaolin was observed before and after its amendment with the XG.

The volume change behavior of kaolin and XGK10 in terms of normalized thickness with 0.5 mol/L $CaCl_2$ as pore-fluid was plotted in Fig. 2H under the mechanical load. A collapse of 12%–13% for the kaolin sample was observed due to the application of the prevailing hydro-mechanical loading conditions. The normalized thickness of the kaolin sample does not increase after initial collapse, which represents the insignificant development of DDLs in $CaCl_2$ salt environment. For XGK10, a slight collapse of approximately 1% was initially observed due to the application of hydro-mechanical load. The sample achieved its original volume within 30 minutes of the start of the experiment, and it started further swelling with time due to the complete formation of XG gel. An equilibrium normalized thickness of 1.08 was achieved with XGK, which represents the overall swelling of the sample. The swelling of XGK10 is thus taking place due to the higher osmotic repulsion pressure between the XG gel. The swelling of the sample upon inundation with 0.5 mol/L $CaCl_2$ is attributed to the formation of XG gel. The XG gel interacts with calcium ions due to electrostatic interaction between carboxyl groups in XG and cations.

The dry XG biopolymer is generally found in the coiled structure form (Tian et al., 2019); the presence of the hydroxyl and carboxyl groups on the XG chain attracts water and forms a layer of water around it upon hydration, as shown in Fig. 3A. The swelling of the sample upon inundation with water is attributed to the formation of xanthan gum gel, which can absorb water molecules through electrostatic interaction between a water molecule and carboxyl groups present in XG. The formation of the XG gel upon hydration was confirmed with the FESEM micrograph images, as shown in Fig. 3C. Fig. 3(C.i) shows the micrograph of dry XG, which confirms the coiled structure; moreover, Fig. 3(c.ii) shows the formation of the XG coating. The mechanical force applied is countered by the developed repulsive osmotic forces between the XG-coated kaolin, as shown in Fig. 3B. The formation of the XG coating over kaolin particles was also confirmed with atomic force microscopy (AFM). The AFM morphologies of kaolin and XGK were plotted in Figs. 3D and 3E, respectively. The kaolin particles have a thickness of 0.19 μm as shown in Fig. 3D, which increased to 0.25 μm (Fig. 3E) for the XGK sample. The increase in the height of kaolin particles is attributed to the formation of an XG gel coating over the kaolin surface. The formation of the coating over the kaolin surface is also confirmed in earlier studies (Kwon et al., 2023).

The FESEM micrographs of kaolin and XGK samples permeated with different pore-fluids were presented in Fig. 4. The FESEMs of kaolin and XGK were performed after permeation with distilled water, as Fig. 4A and 4B, respectively. The saturated samples were collected for FESEM from the middle of the compacted clay samples. The kaolin sample shows various water paths in the sample, which contributes to the

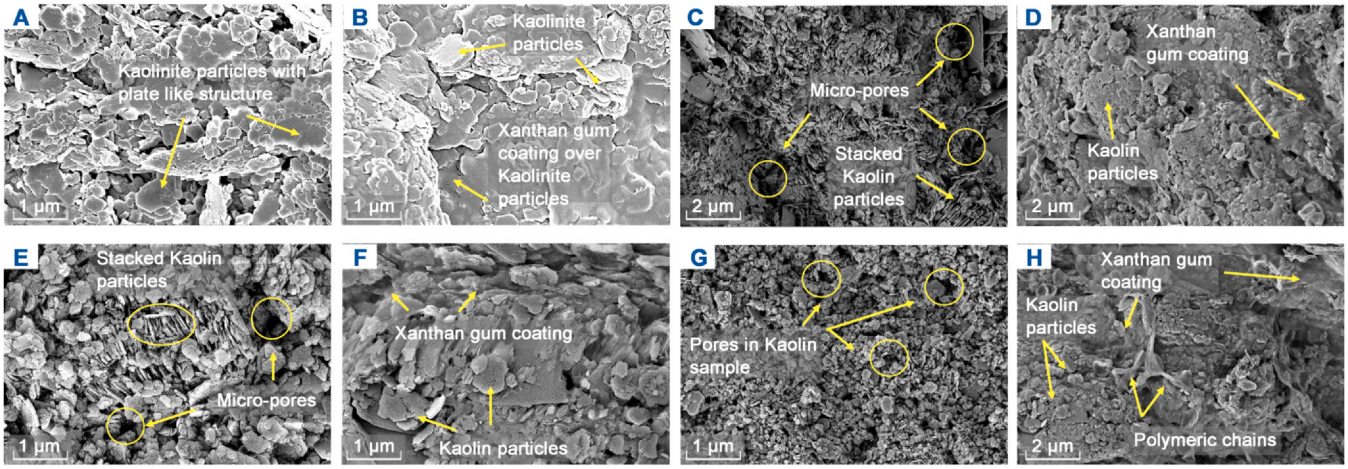


Fig. 4. FESEM micrographs of (**A**) kaolin; (**B**) XGK after permeation with D.W.; (**C**) Kaolin; (**D**) XGK after permeation with 0.5 mol/L NaCl; (**E**) Kaolin; (**F**) XGK after permeation with 0.5 mol/L KCl (**G**) Kaolin; and (**H**) XGK after permeation with $CaCl_2$.

higher hydraulic infiltration of the pore-fluid. The XGK sample shows the coating of the xanthan gum layer over the kaolin particles, and the clogging of the pores of kaolin is also visible in Fig. 4B. The negatively charged side chains of XG and positively charged edges of kaolin directly interact by hydrogen bonds between carboxyl groups of XG and O in kaolin minerals (Kwon et al., 2023). The reason behind the reduction in hydraulic infiltration of XGK is the clogging of pores with xanthan gum gel, as confirmed in Fig. 4B. The FESEMs of kaolin and XGK samples were performed after permeation with 0.5 M NaCl as shown in Fig. 4C and 4D, respectively. The kaolin sample shows various water paths in the sample, which contributes to the higher hydraulic infiltration of the pore-fluid. The XGK sample shows the coating of the xanthan gum layer over the kaolin particles, and the clogging of the pores of kaolin is also visible in Fig. 4D. The reason behind the reduction in hydraulic infiltration of XGK is the clogging of pores with xanthan gum gel, as depicted in Fig. 4D. The FESEM of the kaolin and XGK after the permeation of 0.5 mol/L KCl as pore-fluid were presented in Fig. 4E and 4F, respectively. The kaolin sample showed micro-pores present in it, which contributed to the higher hydraulic infiltration of the pore fluid. The XGK samples showed the presence of the XG gel, which contributes to the clogging of the pores in the sample as visible in Fig. 4F. The FESEMs of kaolin and XGK were performed after permeation with 0.5 mol/L $CaCl_2$ as pore-fluid in Fig. 4G and 4(H, respectively. The kaolin sample shows various water paths in the sample, which contributes to the higher hydraulic infiltration of the pore-fluid. The XGK sample shows the coating of the xanthan gum layer over the kaolin particles, and the clogging of the pores of kaolin is also visible in Fig. 4H. The reason behind the reduction in hydraulic infiltration of XGK is the clogging of pores with XG gel. The rate of reduction of hydraulic infiltration is quick in alone kaolin as compared to XGK, because the breaking of the card-house structure does not take much time as compared to the formation of XG gel. This is also a reason for the higher hydraulic infiltration of the XGK sample around 20 minutes after the start of the experiment.

The elemental analysis of samples was performed using energy-dispersive X-ray (EDX) spectroscopy and presented in Fig. 5. The adsorption potential of the XGK layer for cations was evaluated using EDX. The spectra of pure kaolin and pure XG were presented as Fig. 5A and 5B. Both kaolin and XG sample spectra show the absence of sodium, potassium, and calcium. The sodium is present as one of the major elements in the XGK sample permeated with NaCl as shown in Fig. 5C. The potassium is found to be present in the XGK sample permeated with KCl as pore-fluid as shown in Fig. 5D. Further, the calcium was present in the XGK sample permeated with $CaCl_2$ solution and EDX was presented in Fig. 5E. Therefore, the EDX spectra results confirm the adsorption potential of the XGK sample for the different cations upon permeation and its ability to arrest these ions.

The N_2 gas adsorption and desorption experiments on kaolin and XGK samples were conducted to evaluate the BET surface area and pore size distribution as presented in Fig. 6. The sorption-desorption isotherms were shown in Fig. 6A, and the highest adsorption was found at a relative pressure (P/P_0) of 0.95–1 (Atinafu et al., 2020; Bordoloi et al., 2022). The surface area of the XGK sample was found to be 18.89 m^2/g, which is quite higher than the surface area of bare kaolin (i.e., 11 m^2/g). The higher specific surface area was found for the XGK sample due to the smaller pore size as compared to kaolin. The smaller pore size of XGK is due to the pore-clogging due to XG gel formation. The pore size distribution of kaolin and XGK samples was presented in Fig. 6B. Most of the pores of kaolin and XGK were found to be smaller than 10 nm, while the largest pores of 102 and 113 nm were found for kaolin and XGK samples, respectively. More pores of smaller size were dominant in the XGK sample, while kaolin has more pores of larger size.

The kaolin clay compacted in a dry state has an open card-house-type structure due to the edge–edge interactions. The hydration of kaolin with water alters the charges on its edges from positive to negative (Choudhury & Bharat, 2018), which further leads to the breaking of the card-house type structure as illustrated in Fig. 6C and D. The observation of a significant reduction in the volume of the kaolin along with hydraulic infiltration is attributed to the same reason. However, the alone kaolin at lower density does not have significant development of diffused double layers to achieve the limiting value of hydraulic conductivity ($< 10^{-9}$ m/s). The saturated hydraulic conductivity of the bare kaolin is also governed by the hydrated radius of the cation in pore fluid. The saturated hydraulic infiltration was found to be lowest for the Na^+ ions solution due to the highest hydrated radius of sodium as compared to potassium. The XGK before and after hydration shown in Fig. 6E and 6F respectively. The macro-voids present in kaolin samples are reduced due to the breaking of card-house structure as well as the clogging of pores with xanthan gum gel. The coating of the XG over kaolin restricts the movement of pore fluid across it. Due to the presence of many carboxyl groups, the XG gel has the potential to the cations. Adsorption of cations on the XG surface and clog formations are the main mechanisms for lower hydraulic infiltration of different pore fluids across the tailing barriers.

The sealing time for XGK with distilled water was found to be higher (510 min.) than other pore-fluids, and it was found to be lowest (270 min.) for calcium ions (Ca^{2+}). The sealing time for monovalent cations (i.e., Na^+, and K^+) was found to be almost the same, i.e., (360–380 min.). Calcium ions act as cross-linkers between polymeric chains of XG, which reduces the sealing time. Monovalent cations show

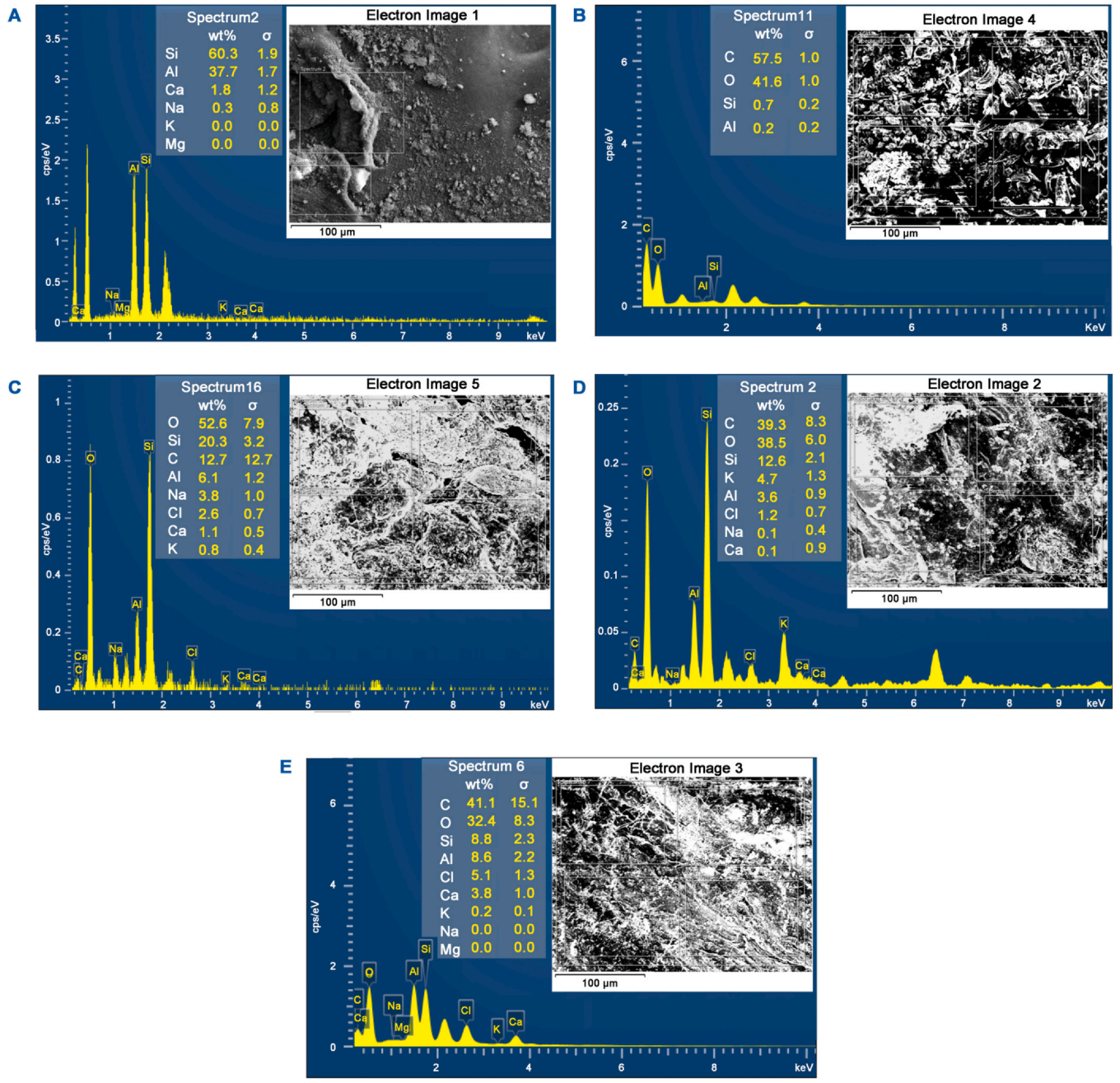


Fig. 5. EDX spectra of (**A**) pure kaolin; (**B**) pure xanthan gum; and XGK after permeation with (**C**) NaCl; (**D**) KCl; (**E**) $CaCl_2$ as pore-fluid.

a slightly higher sealing time than divalent cations due to a reduction in cross-linking. The highest sealing time of water is attributed to the absence of crosslinking in XG.

4.2. Diffusion rates of salts through kaolin and XG amended kaolin

Through-diffusion experiments were conducted for three different salts having a 0.5 mol/L initial concentration in the source reservoir. The saturated kaolin and XGK samples were placed in different diffusion cells, and reservoirs were attached to either end of the diffusion cell. The test was started by placing a 0.5 mol/L salt solution on the source side and distilled water on the collector side. The samples were collected and analyzed for the presence of inorganic ions at different time intervals up to 60 days. The temporal variations of relative concentrations of measured source and collector reservoirs for the NaCl diffusion experiment with kaolin were presented in Fig. 7A. The temporal variations in relative concentrations of ions in both reservoirs for XGK with 0.5 mol/L NaCl solution as an initial concentration in the source reservoir were presented in Fig. 7B. The concentrations in the source reservoir decreased with time and increased in the collector reservoir for both kaolin and XGK. A relative concentration of 0.073 and 0.089 was observed after 60 days in the collector reservoir for kaolin and XGK, respectively, with NaCl solution. The diffusion coefficient and retardation factors were evaluated by minimizing the error between measured and theoretical concentration profiles obtained by solving Eqs. (2–6), and optimization (Bharat et al., 2009; Bharat, 2013). The theoretical profiles for source and collector reservoirs were also presented in Fig. 7A and 7B for kaolin and XGK, respectively. The diffusion coefficient and retardation factor of kaolin with NaCl solution were found to be 1.41×10^{-10} m^2/s and 18.69, respectively. These values were reduced to 1.09×10^{-10} m^2/s and 14.05, respectively, for NaCl solution upon amendment of kaolin with XG. The theoretical

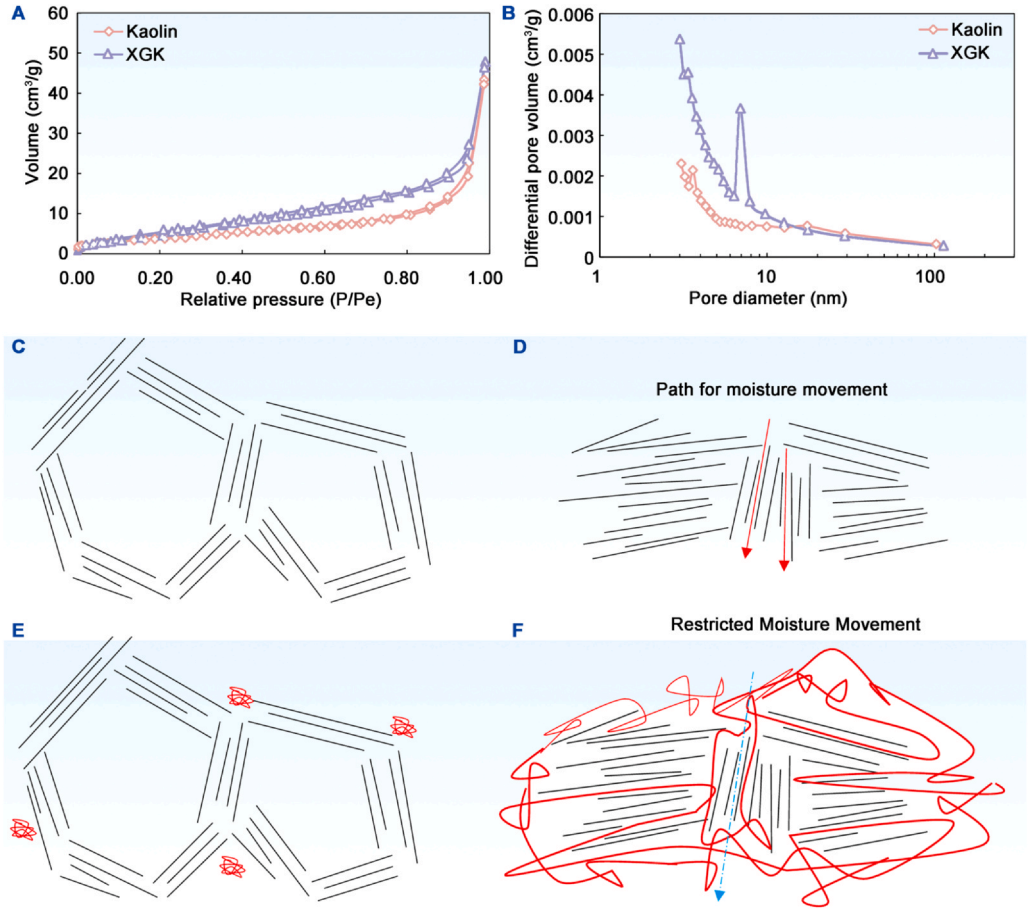


Fig. 6. (**A**) Nitrogen gas adsorption desorption isotherm, and (**B**) pore size distribution, for kaolin and XGK samples; (**C**) Illustration showing open card-house structure in dry compacted sample; (**D**) Face – face orientation of kaolin particles after inundation; (**E**) Dry kaolin sample with coiled xanthan gum particles; (**F**) Xanthan gum gel formation around the kaolin particles with restricted moisture movement.

profiles for kaolin and XGK with NaCl salt solution showed a very good theoretical estimation with a root mean square error (RMSE) value of 0.0199 and 0.0132, respectively.

The temporal variations of relative concentrations of measured source and collector reservoirs for the KCl diffusion experiment with kaolin and XGK were presented in Fig. 7C and 7D, respectively. The relative concentrations in the source reservoir decreased with time and increased in the collector reservoir for both kaolin and XGK. A relative concentration of 0.048 and 0.14 was observed after 60 days in the collector reservoir for kaolin and XGK, respectively with KCl salt solution. The diffusion coefficient and retardation factors were evaluated by minimizing the error between measured and theoretical concentration profiles obtained by solving the Eqs. (2–6), using optimization. The theoretical profiles for source and collector reservoirs were also presented in Fig. 7C and 7D for kaolin and XGK, respectively. The diffusion coefficient and retardation factor of kaolin with KCl solution were found to be 1.61×10^{-10} m^2/s and 9.36, respectively. These values were changed to 7.44×10^{-11} m^2/s and 12.82, respectively, for KCl solution upon amendment of kaolin with XG. The theoretical profiles for kaolin and XGK with KCl salt solution showed a very good theoretical estimation with an RMSE value of 0.0195 and 0.0151, respectively.

The temporal variations of relative concentrations of measured source and collector reservoirs for the $CaCl_2$ diffusion experiment with kaolin and XGK were presented in Fig. 7E and 7F, respectively. The concentrations of $CaCl_2$ in the source reservoir decreased with time and increased in the collector reservoir for both kaolin and XGK. A relative concentration of 0.09 and 0.18 were observed after 60 days in the collector reservoir for kaolin and XGK, respectively, with $CaCl_2$ salt solution. The diffusion coefficient and retardation factors were evaluated by minimizing the error between measured and theoretical concentration profiles obtained by solving Eqs. (2–6) and using optimization (Bharat et al., 2009; Bharat, 2013). The theoretical profiles for source and collector reservoirs were also presented in Fig. 7E and 7F for kaolin and XGK, respectively. The theoretical profiles for kaolin and XGK with $CaCl_2$ salt solution showed very good fitting with RMSE values of 0.0239 and 0.0163, respectively. The diffusion coefficient and retardation factor of kaolin with $CaCl_2$ solution were found to be 1.92×10^{-10} m^2/s and 11.62, respectively. These values were reduced to 8.36×10^{-11} m^2/s and 7.69, respectively, for $CaCl_2$ solution upon amendment of kaolin with XG. The values of the diffusion coefficient and retardation factor for three different salts through kaolin and XGK were also tabulated in Table 2.

The diffusion values obtained in the study were compared to the literature and shown in Table 3. The D_e values were found to be similar to the values obtained by (Kau et al., 1999; Mon et al., 2016) due to the similar density of the kaolin as in the present work. Moreover, the method used by these researchers is also the same. Whereas, high diffusion and lower R_d as compared to the present work were observed by Shackelford et al. (Shackelford et al., 1989). Such differences in the values can be due to the errors involved in destructive technique of In-diffusion techniques. Further, the difference in quality of kaolin can also result in some variation in values. In general, the results obtained in the present study are in good agreement with the literature.

The difference in the values of the D_e and R_d for similar test conditions with different salts is expected due to the change in the hydrated radius of the cations. The larger hydrated radius of the cations cannot pass through the smaller pores and hence may not significantly

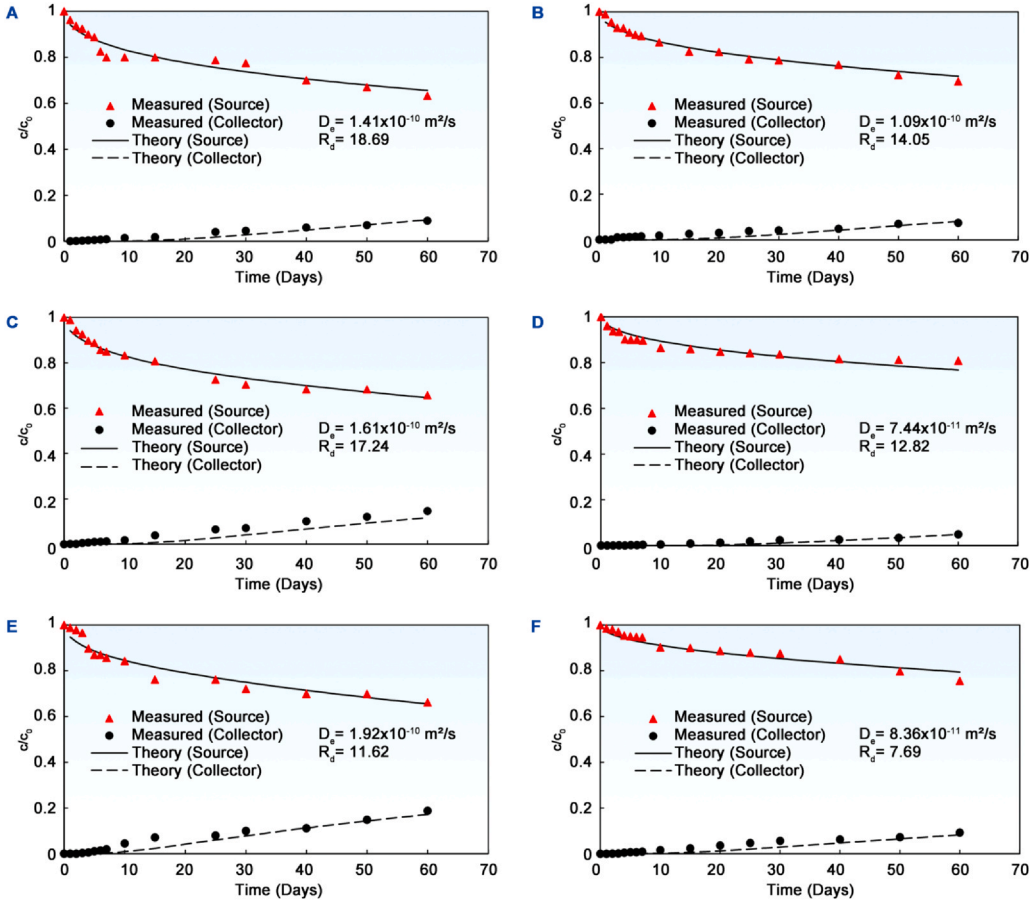


Fig. 7. Comparison of experimental measured and theoretical profile at source and collector reservoir for Kaolin with (**A**) 0.5 mol/L NaCl, (**C**) 0.5 mol/L KCl, and (**E**) 0.5 mol/L $CaCl_2$; and XGK with (**B**) 0.5 mol/L NaCl, (**D**) 0.5 mol/L KCl, and (**F**) 0.5 mol/L $CaCl_2$.

Table 2
The diffusion coefficient and retardation factor for kaolin and XG amended kaolin with different salts.

Material	Pore fluid	Effective diffusion Coefficient, D_e	Retardation factor, R_d	Root mean square error, RMSE
Kaolin	0.5 mol/L NaCl	1.41×10^{-10} m^2/s	18.69	0.02
	0.5 mol/L KCl	1.61×10^{-10} m^2/s	9.36	0.0195
	0.5 mol/L $CaCl_2$	1.92×10^{-10} m^2/s	11.62	0.024
XG amended Kaolin	0.5 mol/L NaCl	1.09×10^{-10} m^2/s	14.05	0.013
	0.5 mol/L KCl	7.44×10^{-11} m^2/s	12.82	0.015
	0.5 mol/L $CaCl_2$	8.36×10^{-11} m^2/s	7.69	0.016

Table 3
Comparison of the diffusion coefficient and retardation factor for different contaminants through compacted kaolin.

Contaminant	Density (g/cm^3)	Porosity	$D_e \times 10^{-10}$ m^2/s	R_d	Method	Reference
K^+	1.272	0.52	13.9	3.95	In-diffusion for D_e and Batch Sorption for R_d	(Shackelford et al., 1989)
Cd^{2+}	1.272	0.52	4.8	2.04		
Zn^{2+}	1.272	0.52	9.1	3.15		
^{86}Rb	-	-	2.4*	-	Half-cell method	(Phillips & Brown, 1964).
Floride	1.1	0.57	3.488–6.976	61–110	Through diffusion test	(Kau et al., 1999)
K^+	1	0.60	1.55*	-	Solute diffusion test	(Mon et al., 2016)
	1.2	0.53	1.25*	-		
Cl^-	1	0.60	1.70*	-		
	1.2	0.53	1.10*	-		
K^+	1.7	0.35	8.2	5.8	Through Diffusion Test	(Das & Bharat, 2017)
Na^+	1.2	0.54	1.41	18.69	Through Diffusion Test	Present Work
K^+	1.2	0.54	1.61	9.36		
Ca^{2+}	1.2	0.54	1.92	11.62		

* Apparent diffusion coefficient.

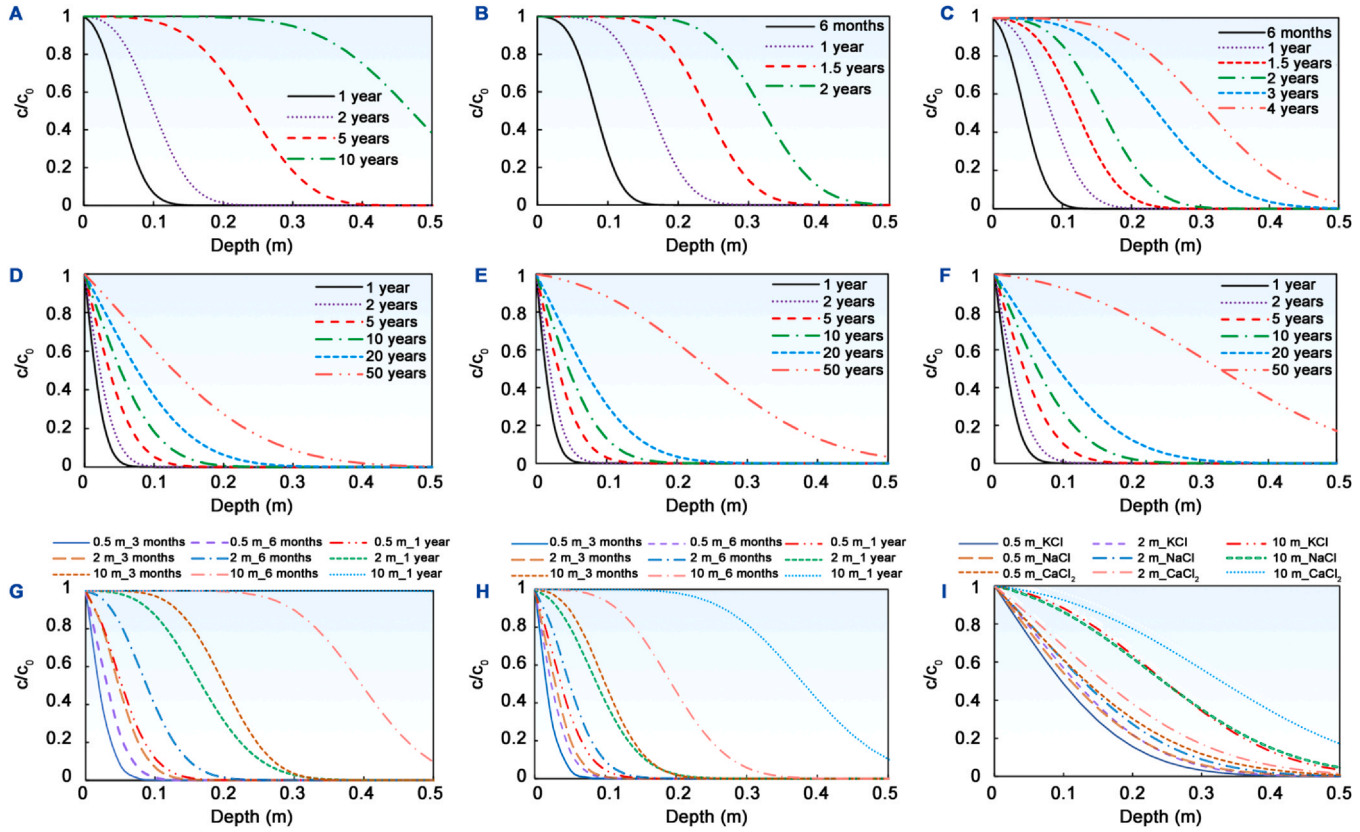


Fig. 8. Contaminant migration profiles with time for (**A**) 0.5 mol/L NaCl; (**B**) 0.5 mol/L KCl; (**C**) and 0.5 mol/L $CaCl_2$ through kaolin; (**D**) 0.5 mol/L NaCl; (**E**) 0.5 mol/L KCl; and (**F**) 0.5 mol/L $CaCl_2$ through XGK; Contaminant profiles of different hydraulic head of leachate for (**G**) 0.5 mol/L KCl through kaolin with time; (**H**) 0.5 mol/L $CaCl_2$ through kaolin with time; and (**I**) XGK with different pore-fluid for 50 years' time duration.

contribute to the diffusion process. The same can be said for the lowest value of diffusion coefficient for sodium as compared to potassium and calcium; sodium has the largest hydrated radius as compared to the other cations. Further, the differences in the retardation factor are attributed to the sorption ability of these cations on the kaolin clay. The sorption ability of the kaolin will depend on various physico-chemical forces between the particles. The interactions of the cations with the kaolin show contrast behavior as that of bentonite. The equilibrium sediment volume of kaolin clay shows an order of $K^+ > Ca^{2+} > Na^+$, whereas bentonites show the opposite behavior $Na^+ > Ca^{2+} > K^+$. Such behavior of kaolin is observed due to the dispersed nature of kaolin in the presence of K^+ as compared to Na^+ (Sridharan & Prakash, 1999). The flocculated structure of kaolin in the presence of the K^+ as compared to Na^+ will dominate positive charges on its termination sites, leading to lower retention of K^+. Moreover, the dispersed structure of the kaolin with the Na^+ will have more negatively charged termination sites as compared to K^+, which leads to higher retention of the Na^+ ion and hence a higher R_d.

5. Numerical simulation of contaminant through barriers for evaluating design period

The attenuation ability of the cations is based on the evaluated model parameters (K_s, D_e, and R_d) of the engineered barrier facilities. The contaminant migration through barriers is mainly governed by the advection-diffusion equation. After evaluating independent advection (saturated hydraulic conductivity) and diffusion (effective diffusion coefficient and retardation factor) characteristics, the transport of contaminants was simulated in a 500 mm-thick kaolin clay layer as well as the XGK layer. The normalized concentration distribution for the studied contaminants was given at different periods in Fig. 8. The migration of contaminants for kaolin alone was mainly governed by advection, whereas diffusion was the dominant phenomenon in XGK. A kaolin layer of 500 mm thickness attenuates the migration of sodium cations for up to 10 years. Moreover, the XGK layer of the same thickness can attenuate sodium ions for more than 50 years, as shown in Fig. 8A and 8D. The migration of potassium through the kaolin layer attenuates the contaminant for less than 5 years; further, the XGK improved the migration rates by decreasing the saturated hydraulic conductivity to less than 10^{-9} m/s and the effective diffusion coefficient to a smaller value. Thus, the XGK attenuates potassium for more than 50 years, as shown in Fig. 8B and 8E. Similarly, the 500 mm thick layer of kaolin attenuates the migration of calcium for up to 5–10 years, which improves significantly after kaolin is amended with XG, and the 500 mm thick XGK layer attenuates the calcium ion migration for more than 50 years as shown in Fig. 8C and 8F.

The hydraulic head of leachate also influences the migration of contaminants through barrier material. The concentration profiles of 0.5 mol/L KCl for a 500 mm-thick kaolin layer for different hydraulic heads were plotted in Fig. 8G. The plotted profiles showed that the hydraulic head significantly influenced the contaminant profiles. The lowest hydraulic head (i.e., 1 m) showed a migration of 200 mm in 1 year, while the 10-meter hydraulic head showed the failure of the barrier after 1 year. The concentration profiles of 0.5 mol/L $CaCl_2$ for 500 mm-thick kaolin layer for three different hydraulic heads were plotted in Fig. 8H. The calcium migration also showed similar results as that of potassium; the barrier system showed very less migration of calcium at the lower head. The barrier system started failing after 1 year and showed rapid migration of calcium at a hydraulic head of 10 m. The contaminant profiles of three different contaminants for a 500 mm-thick XGK layer with different hydraulic heads for 50 years were plotted in Fig. 8I. The migration profiles after 50 years did not change significantly with hydraulic heads. Moreover, hydraulic heads of 10 m for all contaminants showed higher migration as compared to lower heads. The calcium ion showed higher migration when compared

with the other two cations. For all three contaminants, a 500 mm layer of XGK is sufficient to act as a barrier for more than 50 years. Based on the concentration profiles with different cations for the XGK layer evaluated design time was found to be 50 years.

6. Conclusions

The study on the engineered barriers for tailing disposal facilities was conducted using permeation experiments and through-diffusion experiments. The following conclusions were drawn from the study:

- Although some recent studies (Das & Bharat, 2021) suggested the use of natural kaolin for barrier applications along with the GB, the hydraulic performance of kaolin was not satisfactory at smaller compaction densities due to significantly higher hydraulic infiltration rates when compared to the limiting saturated hydraulic conductivity. An insufficient osmotic ability was developed in the presence of the studied pore fluids under lower compaction density.
- The XG-amended kaolin achieved hydraulic infiltration rates lower than the limiting saturated hydraulic conductivity. The formation of XG gel and the coating of this gel over kaolin particles led to the lowering of hydraulic infiltration rates. The swelling of the XG chains upon hydration under the influence of ionic salt solutions due to the negative charge in the carboxyl groups reduced the permeation rates significantly. The cross-linking of XG chains with positive charge cations further helped in the reduction in hydraulic infiltration rates, which is evident from the lower sealing time in the presence of divalent cations as compared to the monovalent cations, as well as FESEM micrographs.
- The immediate reduction in the fluid permeation rates, as well as the collapse of kaolin upon inundation, is attributed to the breakage of the card-house structure.
- The diffusion coefficient of kaolin decreased significantly for all the studied high-ionic-strength salts after amendment with XG due to the less availability of the void space with the formation of the gel.
- The role of the type of cations on diffusion coefficients is governed by the hydrated radii of cations. The larger hydrated radius of the cations cannot pass through the smaller pores and hence may not significantly contribute to the diffusion process. The same can be said for the lowest value of diffusion coefficient for sodium as compared to potassium and calcium.
- Further, the differences in the retardation factor are attributed to the sorption ability of these cations on the kaolin clay. The flocculated structure of kaolin in the presence of the K^+ as compared to Na^+ will dominate positive charges on its termination sites, leading to lower retention of K^+, which leads to higher retention of the Na^+ ion and hence a higher R_d.
- The hydraulic head of the tailing disposal facility also plays an important role in contaminant migration through kaolin. The higher hydraulic heads of kaolin were found to be more critical as compared to the lower heads. The hydraulic head did not play a significant role in contaminant migration through XGK, as contaminant migration is governed by the low diffusion mechanism in such cases.
- The XGK liners can be utilized in regions having a large presence of kaolin clay and an absence of bentonite. A 500 mm thick XGK is sufficient as a barrier in tailing disposal facilities for containing all different wastes for more than 50 years, as the sealing ability is critical only with high ionic strength salts.

CRediT authorship contribution statement

Bharat Venkata Tadikonda: Writing – review & editing, Validation, Supervision, Software, Resources, Project administration, Methodology, Investigation, Formal analysis, Conceptualization. **Himanshu Yadav:** Writing – original draft, Visualization, Software, Methodology, Investigation, Formal analysis, Data curation, Conceptualization.

Funding

The authors thank Science and Engineering Research Board, (CRG/2021/000783), the Department of Science and Technology, Government of India, for funding this research project. The authors are also thankful to the Clay Mineral Society, U.S.A., for student research grant to H.Y.

Data availability

All the experimental data used in the study will appear in the manuscript. The code used in the study can be provided upon request to the corresponding author.

Declaration of Competing Interest

The authors declare that they have no known competing financial interests or personal relationships that could have appeared to influence the work reported in this paper.

Acknowledgements

The authors acknowledge the support from the FESEM, Surface area and Pore Size analysis, AFM, and EDX facility, Central Instrument Facility, Indian Institute of Technology Guwahati for the microstructural analysis of samples.

References

Abreu, M. M., Matias, M. J., Magalhães, M. C., & Basto, M. J. (2016). Impacts on water, soil and plants from the abandoned Miguel vacas copper mine, Portugal. *Journal of Geochemical Exploration, 96*(2–3), 161–170. https://doi.org/10.1016/j.gexplo.2007.04.012

Adhikary, P., & Singh, R. P. (2004). Synthesis, characterization, and flocculation characteristics of hydrolyzed and unhydrolyzed polyacrylamide grafted xanthan gum. *Journal of Applied Polymer Science, 94*, 1411–1419. https://doi.org/10.1002/app.21040

Akhila, V., & Bharat, T. V. (2022). Prediction of hydraulic conductivity parameters of slurries from centrifuge consolidation settlements. *Canadian Geotechnical Journal*. https://doi.org/10.1139/cgj-2021-0700

Amulya, K., Katakojwala, R., Ramakrishna, S., & Mohan, S. V. (2021). Low carbon biodegradable polymer matrices for sustainable future. *Composites Part C Open Access, 4*(2021), Article 100111. https://doi.org/10.1016/j.jcomc.2021.100111

Anam, A., Gamit, N., Prajapati, V., & Dholakiya, B. Z. (2023). An overview of kaolin and its potential application in thermosetting polymers. *Materials Today Communications, 36*, Article 106827. https://doi.org/10.1016/j.mtcomm.2023.106827

ASTM standard D4318–10 (2010). *Standard test methods for liquid limit, plastic limit, and plasticity index of soils.* West Conshohocken: American Society for Testing and Materials.

Atinafu, D. G., Jin Chang, S., Kim, K. H., & Kim, S. (2020). Tuning surface functionality of standard biochars and the resulting uplift capacity of loading/energy storage for organic phase change materials. *Chemical Engineering Journal, 394*, Article 125049. https://doi.org/10.1016/j.cej.2020.125049

Benson, C. H., Zhai, H., & Wang, X. (1994). Estimating hydraulic conductivity of compacted clay liners. *Journal of Geotechnical and Geoenvironmental Engineering, 120*(2), 366–387. https://doi.org/10.1061/(ASCE)0733-9410(1994)120:2(366)

Bharat, T. V. (2013). Analytical model for 1-D contamination diffusion through clay barriers. *Environmental Geotechnics, 1*(EG4), 210–221. https://doi.org/10.1680/envgeo.13.00035

Bharat, T. V., Sivapullaiah, P. V., & Allam, M. M. (2009). Swarm intelligence - based solver for parameter eastimation of laboratory through diffusion transport of contaminants. *Computers and Geotechnics, 36*, 984–992. https://doi.org/10.1016/j.compgeo.2009.03.006

Biju, M. S., & Arnepalli, D. N. (2020). Effect of biopolymers on permeability of sand-bentonite mixtures. *Journal of Rock Mechanics and Geotechnical Engineering, 12*(5), 1093–1102. https://doi.org/10.1016/j.jrmge.2020.02.004

Bordoloi, U., Das, D., Kashyap, D., Patwa, D., Bora, P., Muigai, H. H., & Kalita, P. (2022). Synthesis and comparative analysis of biochar based form-stable phase change materials for thermal management of buildings. *Journal of Energy Storage, 55*, Article 105801. https://doi.org/10.1016/j.est.2022.105801

Bozyigit, I. (2025). Strength properties of clay treated with fiber and biopolymer subject to freeze–thaw conditions. *Journal of Materials in Civil Engineering, 37*(5), Article 04025090. https://doi.org/10.1061/JMCEE7.MTENG-19201

Bozyigit, I., Zingil, H. O., & Altun, S. (2023). Performance of eco-friendly polymers for soil stabilization and their resistance to freeze–thaw action. *Construction and Building Materials, 379*, Article 131133. https://doi.org/10.1016/j.conbuildmat.2023.131133

Cadmus, M. C., Jackson, L. K., Burton, K. A., Plattner, R. D., & Slodki, M. E. (1982). Biodegradation of xanthan gum by Bacillus sp. *Applied and Environmental Microbiology, 44*(1), 5–11. https://doi.org/10.1128/aem.44.1.5-11.1982

Celik, M. S. (2004). Electrokinetic behavior of clay surfaces. *Interface Science and Technology, 1*, 57–89. https://doi.org/10.1016/S1573-4285(04)80037-1

Chakraborty, S., Dutta, B., Ghosh, N., Halder, S., Chatterjee, R., Sengupta, S., ... Bandyopadhyay, A. (2023). Strategic grafting of poly METAC and polyacrylamide onto xanthan gum for flocculating kaolin at lower concentration. *Materials Today Communications, 34*, Article 105091. https://doi.org/10.1016/j.mtcomm.2022.105091

Chang, I., Im, J., Prasidhi, A. K., & Cho, G. C. (2015). Effects of Xanthan gum biopolymer on soil strengthening. *Construction and Building Materials, 74*, 65–72. https://doi.org/10.1016/j.conbuildmat.2014.10.026

Chapman, H.D., (1965). Cation-exchange capacity. In: Black, C.A. (Ed.), Methods of Soil Analysis - Chemical and Microbiological Properties. Agronomy. vol. 9, pp. 891–901.

Chen, J., Salihoglu, H., Benson, C. H., Likos, W. J., & Edil, T. B. (2019). Hydraulic conductivity of bentonite–polymer composite geosynthetic clay liners permeated with coal combustion product leachates. *Journal of Geotechnical and Geoenvironmental Engineering, 145*(9), 04019038. https://doi.org/10.1061/(ASCE)GT.1943-5606.0002105

Choi, H.-J., Nguyen, T.-B., Lim, J., & Choi, H. (2015). Parametric study on cutoff performance of soil-bentonite slurry wall: Consideration of construction defects and bentonite cake. *KSCE Journal of Civil Engineering, 19*(6), 1681–1692. https://doi.org/10.1007/s12205-014-1171-1

Choudhury, C., & Bharat, T. V. (2018). Wetting-induced collapse behavior of kaolinite: Influence of fabric and inundation pressure. *Canadian Geotechnical Journal, 55*(7), 956–967. https://doi.org/10.1139/cgj-2017-0297

Christian, W., & Tarek, A. (2021). Investigating factors influencing polymer elution and the mechanism controlling the chemical compatibility of GCLs containing linear polymers. *Geotextiles and Geomembranes, 49*(4), 1004–1018. https://doi.org/10.1016/j.geotexmem.2021.01.009

Concas, A., Ardau, C., Cristini, A., Zuddas, P., & Cao, G. (2006). Mobility of heavy metals from tailings to stream waters in a mining activity contaminated site. *Chemosphere, 63*(2), 244–253. https://doi.org/10.1016/j.chemosphere.2005.08.024

Darde, B., Roux, J.-N., Pereira, J.-M., Dangla, P., Talandier, J., Vu, M. N., & Tang, A. M. (2021). Investigating the hydro-mechanical behaviour of bentonite pellets by swelling pressure tests and discrete element modelling. *Acta Geotechnica, 16*, 507–524. https://doi.org/10.1007/s11440-020-01040-5

Das, P., & Bharat, T. V. (2017). Effect of counter ions on the diffusion characteristics of a compacted bentonite. *Indian Geotechnical Journal, 47*(4), 477–484. https://doi.org/10.1007/s40098-017-0241-y

Das, P., & Bharat, T. V. (2021). Kaolin based protective barrier in municipal landfills against adverse chemo – mechanical loadings. *Scientific Reports, 11*, Article 10354. https://doi.org/10.1038/s41598-021-89787-z

Dehghan, H., Tabarsa, A., Latifi, N., & Bagheri, Y. (2019). Use of xanthan and guar gums in soil strengthening. *Clean Technologies and Environmental Policy, 21*(1), 155–165. https://doi.org/10.1007/s10098-018-1625-0

Devlin, J., & Parker, B. (1996). Optimum hydraulic conductivity to limit contaminant flux through cutoff walls. *Ground Water, 34*(4), 719–726. https://doi.org/10.1111/j.1745-6584.1996.tb02060.x

Ding, H., & Geng, X. (2025). Strength and Durability Performance of Sandy Loam Reinforced with Xanthan Gum and Biochar. *Journal of Materials in Civil Engineering, 37*(2), Article 04024515. https://doi.org/10.1061/JMCEE7.MTENG-18508

Elkafoury, A., & Azzam, W. (2021). Utilize Xanthan gum for enhancing CBR value of used cooking oil-contaminated fine sand subgrade soil for pavement structures. *Innovative Infrastructure Solutions, 6*, 25. https://doi.org/10.1007/s41062-020-00389-6

Elkenawy, M., Gabr, A., & Arab, M. G. (2023). Mechanical properties of unsaturated expansive soils treated with eco-friendly sodium alginate biopolymer. *International Journal of Geosynthetics and Ground Engineering, 9*(3), 34. https://doi.org/10.1007/s40891-023-00452-z

El-Sherbiny, I. M., Abdel-Hamid, M. I., Rashad, M., Ali, A. S., & Azab, Y. A. (2013). New calcareous soil–alginate composites for efficient uptake of Fe (III), Mn (II) and As (V) from water. *Carbohydrate Polymers, 96*(2), 450–459. https://doi.org/10.1016/j.carbpol.2013.04.021

Farmaki, S., Vorrisi, E., Karakasi, O. K., & Moutsatsou, A. (2018). Effect of limestone and dolomite tailings' particle size on potentially toxic elements adsorption. *Open Geoscience, 10*(1), 726–739. https://doi.org/10.1515/geo-2018-0058

Fu, X. L., Shen, S. Q., Reddy, K. R., Yang, Y. L., & Du, Y. J. (2022). Hydraulic conductivity of sand/biopolymer-amended bentonite backfills in vertical cutoff walls permeated with lead solutions. *Journal of Geotechnical and Geoenvironmental Engineering, 148*(2), 04021186. https://doi.org/10.1061/JGGEFK.GTENG-11321

Gapak, Y., Das, G., Yerramshetty, U., & Bharat, T. V. (2017). Laboratory determination of volumetric shrinkage behavior of bentonites: A critical appraisal. *Applied Clay Science, 137*, 554–566. https://doi.org/10.1016/j.clay.2016.10.038

García-Giménez, R., & Jiménez-Ballesta, R. (2017). Mine tailings influencing soil contamination by potentially toxic elements. *Environmental Earth Sciences, 76*, 51. https://doi.org/10.1007/s12665-016-6376-9

García-Guzmán, P., Medina-Torres, L., Bernad-Bernad, M. J., Calderas, F., & Manero, O. (2023). Study of the cholesterol adsorption and characterization of montmorillonite and bentonite clay. *Materials Today Communications, 35*, Article 105604. https://doi.org/10.1016/j.mtcomm.2023.105604

Grim, R. E. (1959). Physico-chemical properties of soils: clay minerals. *Journal of the Soil Mechanics and Foundation Division, ASCE, 85*(SM2), 1–17. https://doi.org/10.1061/JSFEAQ.0000179

Harwood, J. J., & Koirtyohann, S. R. (1987). Modelling of leachates from dolomitic mine tailings. *Environ Geochem Health, 9*(1), 17–22. https://doi.org/10.1007/BF01811112

Hong, C., & Shackelford, C. (2017). Long-term column testing of zeoliteamended backfills. I: Testing methodology and chemical compatibility. *Journal of Geotechnical and Geoenvironmental Engineering, 143*(9), 04017050. https://doi.org/10.1061/(ASCE)GT.1943-5606.0001734

Hu, S., & Zhang, W. (2023). Effects of copper mining wastewater on the performance of waste-based low-clinker cement mortars. *Materials Today Communications, 37*, Article 107131. https://doi.org/10.1016/j.mtcomm.2023.107131

IS: 2720 (1985) Indian standard methods of test for soils. *Part 5: Determination of liquid and plastic limit*. New Delhi: BIS.

Kau, P. M. H., Binning, P. J., Hitchcock, P. W., & Smith, D. W. (1999). Experimental analysis of fluoride diffusion and sorption in clays. *Journal of Contaminant Hydrology, 36*(1-2), 131–151. https://doi.org/10.1016/S0016-7061(97)00122-5

Kaufhold, S., Baille, W., Schanz, T., & Dohrmann, R. (2015). About differences of swelling pressure dry density relations of compacted bentonites. *Applied Clay Science, 107*, 52–61. https://doi.org/10.1016/j.clay.2015.02.002

Klute, A., and Dinauer, R.C. (Editors). (1986). Methods of soil analysis, Part 1. Phys ical and mineralogical methods. *Number 9 in the series of Agronomy*. Soil Science Society of America, American Society of Agronomy.

Kumar, S. A., & Sujatha, E. R. (2021). An appraisal of the hydro-mechanical behaviour of polysaccharides, xanthan gum, guar gum and β-glucan amended soil. *Carbohydrate Polymers, 265*, Article 118083. https://doi.org/10.1016/j.carbpol.2021.118083

Kwon, Y. M., Chang, I., & Cho, G. C. (2023). Xanthan biopolymer-based soil treatment effect on kaolinite clay fabric and structure using XRD analysis. *Scientific Reports, 13*(1), Article 11666. https://doi.org/10.1038/s41598-023-38844-w

Kwon, Y. M., Kang, S. J., Cho, G. C., & Chang, I. (2023). Effect of microbial biopolymers on the sedimentation behavior of kaolinite. *Geomechanics and Engineering, 33*(2), 121–131. https://doi.org/10.12989/gae.2023.33.2.121

Li, T. K., & Rowe, R. K. (2020). GCL self-healing: Fully penetrating hole/slit hydrated with RO water and 10 mM Ca solution. *Geosynthetics International, 27*(1), 34–47. https://doi.org/10.1680/jgein.19.00054

Mäkinen, J., Marja, S., Mohammad, K., Jan-Eric, S., & Päivi, K. (2020). Bioleaching of cobalt from sulfide mining tailings; a mini-pilot study. ISSN 0304-386X *Hydrometallurgy, 196*, Article 105418. https://doi.org/10.1016/j.hydromet.2020.105418

Malusis, M., Maneval, J., Barben, E., Shackelford, C., & Daniels, E. (2010). Influence of adsorption on phenol transport through soil-bentonite vertical barriers amended with activated carbon. *Journal of Contaminant Hydrology, 116*(1–4), 58–72. https://doi.org/10.1016/j.jconhyd.2010.06.001

Mishra, P. N., Scheuermann, A., Bore, T., & Li, L. (2019). Salinity effects on soil shrinkage characteristic curves of fine-grained geomaterials. *Journal of Rock Mechanics and Geotechnical Engineering, 11*(1), 181–191. https://doi.org/10.1016/j.jrmge.2018.06.008

Mon, E. E., Hamamoto, S., Kawamoto, K., Komatsu, T., & Moldrup, P. (2016). Temperature effects on solute diffusion and adsorption in differently compacted kaolin clay. *Environmental Earth Sciences, 75*, 1–9. https://doi.org/10.1007/s12665-016-5358-2

Ni, J., Zhao, R. J., Chen, J. Q., & Geng, X. Y. (2024). Mechanical and hydraulic characteristics of unvegetated or vegetated loess soils amended with xanthan gum. *Transportation Geotechnics, 48*, Article 101350. https://doi.org/10.1016/j.trgeo.2024.101350

Parviainen, A. (2009). Tailings mineralogy and geochemistry at the abandoned Haveri Au–Cu mine, SW Finland. *Mine Water and Environment, 28*(4), 291–304. https://doi.org/10.1007/s10230-009-0088-2

Peirce, J. J., Sallfors, G., & Murray, L. (1986). Overburden pressures exerted on clay liners. *Journal of Environmental Engineering, 112*(2), 264–279. https://doi.org/10.1061/(ASCE)0733-9372(1986)112:2(280

Phillips, R. E., & Brown, D. A. (1964). Ion diffusion: II. Comparision of apparent self and counter diffusion coefficients. *Soil Science Society Proceedings,* 758–763. https://doi.org/10.2136/sssaj1964.03615995002800060024x

Puppala, A. J., Pedarla, A., Pino, A., & Hoyos, L. R. (2017). Diffused double-layer swell prediction model to better characterize natural expansive clays. *Journal of Engineering Mechanics, 143*(9), Article 04017069. https://doi.org/10.1061/(ASCE)EM.1943-7889.0001292

Rosalam, S., & England, R. (2006). Review of xanthan gum production from unmodified starches by Xanthomonas comprestris sp. *Enzyme and Microbial Technology, 39*(2), 197–207. https://doi.org/10.1016/j.enzmictec.2005.10.019

Ruffing, D., Evans, J., & Coughenour, N. (2018). Soil-bentonite slurry trench cutoff wall longevity. *Geotechnics, 297*, 214–223 doi/10.1061/9780784481608.021.

Sample-Lord, K. M., Ahmed, M., & Malusis, M. A. (2021). Diffusion through soil-bentonite backfill from a constructed vertical cutoff wall. *Soils and Foundations, 61*(2), 429–443. https://doi.org/10.1016/j.sandf.2021.01.002

Setz, M. C., Tian, K., Benson, C. H., & Bradshaw, S. L. (2017). Effect of ammonium on the hydraulic conductivity of geosynthetic clay liners. *Geotextiles and Geomembranes, 45*(6), 655–673. https://doi.org/10.1016/j.geotexmem.2017.08.008

Shackelford, C. D. (1991). Laboratory diffusion testing for waste disposal – A review. *J Contam Hydrol, 7*, 177–217. https://doi.org/10.1016/0169-7722(91)90028-Y

Shackelford, C. D., Daniel, D. E., & Liljestrand, H. M. (1989). Diffusion of inorganic chemical species in compacted clay soil. *Journal of Contaminant Hydrology, 4*(3), 241–273. https://doi.org/10.1016/0169-7722(89)90011-9

Singh, S., Kumar, A., & Sitharam, T. G. (2023). Mechanical, microstructural, and durability properties of soil stabilized with alkali-activated jarofix for road applications. *Journal of Hazardous Toxic and Radioactive Waste, 27*(4), Article 04023020. https://doi.org/10.1061/JHTRBP.HZENG-1236

Sridharan, A., & Prakash, K. (1999). Influence of clay mineralogy and pore medium chemistry on clay sediment formation. *Canadian Geotechnical Journal, 36*(5), 961–966. https://doi.org/10.1139/t99-045

Takai, A., Katsumi, T., Inui, T., & Kamon, M. (2017). Solute transport in soil-bentonite cutoff walls considering chemical diffusion. *In Proceedings of the ninteenth int. conf. on soil mechanics and geotechnical engineering,* 3203–3206.

Tallin, J. E., Pufahl, D. E., & Barbour, S. L. (1990). Waste management schemes of potash mines in Saskatchewan. *Canadian Journal of Civil Engineering, 17*(4), 528–542. https://doi.org/10.1139/l90-061

Tian, K., Likos, W. J., & Benson, C. H. (2019). Polymer elution and hydraulic conductivity of bentonite – polymer composite geosynthetic clay liners. *Journal of Geotechnical and Geoenvironmental Engineering, 145*(10), Article 04019071. https://doi.org/10.1061/(ASCE)GT.1943-5606.0002097

Wan, J., Tang, Z., Liu, Y., Xiao, H., & Wang, H. (2024). Study on the improvement of clay properties by xanthan gum and its application on ecological slope protection engineering. *Environmental Technology, 45*(14), 2762–2775. https://doi.org/10.1080/09593330.2023.2186271

Yadav, H., & Bharat, T. V. (2022). Sealing and volume change behaviour of polymer-amended granular bentonite under extreme chemical loading. *In Geo-Congress 2022,* 199–208. https://doi.org/10.1061/9780784484050.021

Yadav, H., Bharat, T. V., Gaurav, S., & Kumar, S. (2023). Fate and transport of coronavirus surrogate through compacted clays for pathogenic waste disposal. *Langmuir, 39*(23), 8042–8054. https://doi.org/10.1021/acs.langmuir.3c00110

Yadav, H., & Bharat, T. V. (2022). *Bentonite based barriers for protecting offshore monuments from saltwater intrusion. In Geotechnical engineering for the preservation of monuments and historic sites III*. CRC Press1152–1160. https://doi.org/10.1201/9781003308867-92

Yadav, H., Sharma, A., & Bharat, T. V. (2022). *Performance of granular bentonite under the influence of chemical and mechanical loadings. In North-East research conclave*. Singapore: Springer Nature Singapore237–244. https://doi.org/10.1007/978-981-19-8464-8_15

Yadav, H., & Tadikonda, B. V. (2022). The Influence of mechanical granulation process and granular bentonite plasticity on self-sealing and volume change behavior. *Journal of Hazardous, Toxic, and Radioactive Waste, 26*(2), 04022003. https://doi.org/10.1061/(ASCE)HZ.2153-5515.0000688

Yin, S., Shao, Y., Wu, A., Wang, H., Liu, X., & Wang, Y. (2020). A systematic review of paste technology in metal mines for cleaner production in China. *Journal of Cleaner Production, 247*, Article 119590. https://doi.org/10.1016/j.jclepro.2019.119590

Yu, B., El-Zein, A., & Rowe, R. K. (2020). Effect of added polymer on the desiccation and healing of a geosynthetic clay liner subject to thermal gradients. *Geotextiles and Geomembranes, 48*(6), 928–939. https://doi.org/10.1016/j.geotexmem.2020.08.001